2005-04

Final Report

GPS Based Real-Time Tire-Road Friction Coefficient Identification

Research

Technical Report Documentation Page

1. Report No.	2.	3. Recipients Accession No.
MN/RC – 2005-04		

4. Title and Subtitle	5. Report Date
GPS BASED REAL-TIME TIRE-ROAD FRICTION COEFFICIENT IDENTIFICATION	September 2004
	6.

7. Author(s)	8. Performing Organization Report No.
Junmin Wang, Lee Alexander, Rajesh Rajamani	

9. Performing Organization Name and Address	10. Project/Task/Work Unit No.
University of Minnesota Department of Mechanical Engineering 111 Church Street S.E. Minneapolis, Minnesota 55455	11. Contract (C) or Grant (G) No. (c) 81655 (wo) 27

12. Sponsoring Organization Name and Address	13. Type of Report and Period Covered
Minnesota Department of Transportation Research Services Section 395 John Ireland Boulevard Mail Stop 330 St. Paul, Minnesota 55155	Final Report
	14. Sponsoring Agency Code

15. Supplementary Notes

http://www.lrrb.org/PDF/200504.pdf

16. Abstract (Limit: 200 words)

This project concentrates on the development of real- time tire-road friction coefficient estimation systems for snowplows that can reliably estimate different road surface friction levels and quickly detect abrupt changes in friction coefficient. Two types of systems are developed – a vehicle-based system and a wheel-based system. The vehiclebased friction measurement system utilizes vehicle motion measurements from differential GPS and other on-board vehicle sensors. The wheel-based friction measurement system utilizes a redundant wheel that is mounted at a small angle to the longitudinal axis of the vehicle.

Complete technical details on the vehicle-based friction measurement system are presented in this report. Compared to previously published results in literature, the advantage of the vehicle-based system developed here is that it is applicable during both vehicle acceleration and braking and works reliably for a wide range of slip ratios, including high slip conditions. The system can be utilized on front/rear-wheel drive as well as all-wheel drive vehicles. Extensive results are presented from experimental results conducted on various surfaces with a winter maintenance vehicle called the "SAFEPLOW." The experimental results show that the system performs reliably and quickly in estimating friction coefficient on different road surfaces during various vehicle maneuvers.

17. Document Analysis/Descriptors		18.Availability Statement
GPS Tire Road	Friction SAFEPLOW	No restrictions. Document available from: National Technical Information Services, Springfield, Virginia 22161

19. Security Class (this report)	20. Security Class (this page)	21. No. of Pages	22. Price
Unclassified	Unclassified	92	

GPS BASED REAL-TIME TIRE-ROAD FRICTION COEFFICIENT IDENTIFICATION

Final Report

Prepared by:

Junmin Wang
Lee Alexander
Rajesh Rajamani
Department of Mechanical Engineering
University of Minnesota

September 2004

Published by:
Minnesota Department of Transportation
Office of Research Services, MS 330
395 John Ireland Boulevard
St. Paul, MN 55155

Acknowledgements

This research was funded by the Minnesota Department of Transportation (Contract No. 81655) and by the ITS Institute, University of Minnesota. We are grateful to John Scharffbillig for his expertise in driving the snowplow, especially on the skid pad.

Table of Contents

List of Figures

List of Tables

Executive Summary

This project concentrates on the development of real-time tire-road friction coefficient estimation systems for snowplows that can reliably estimate different road surface friction levels and quickly detect abrupt changes in friction coefficient. Two types of systems are developed – a vehicle-based system and a wheel-based system. The vehicle-based friction measurement system utilizes vehicle motion measurements from differential GPS and other on-board vehicle sensors. The wheel-based friction measurement system utilizes a redundant wheel that is mounted at a small angle to the longitudinal axis of the vehicle.

Complete technical details on the vehicle-based friction measurement system are presented in this report. Compared to previously published results in literature, the advantage of the vehicle-based system developed here is that it is applicable during both vehicle acceleration and braking and works reliably for a wide range of slip ratios, including high slip conditions. The system can be utilized on front/rear-wheel drive as well as all-wheel drive vehicles. Extensive results are presented from experimental results conducted on various surfaces with a winter maintenance vehicle called the "SAFEPLOW." The experimental results show that the system performs reliably and quickly in estimating friction coefficient on different road surfaces during various vehicle maneuvers.

The new wheel-based system developed in this project has several advantages compared to the popular Norse-meter which is a commercially available redundant wheel-based system. The new wheel-based system has very few moving parts, requires no actuators for skidding the wheel and requires no braking of the wheel. It is expected to be more reliable and much less expensive than the Norsemeter. Experimental results presented in this report show that the new wheel-based system works effectively in determining friction coefficient and in measuring the change of friction coefficient during transition from one type of surface to another.

The developed friction identification systems have many applications in vehicle safety systems such as ABS, skid control and collision avoidance systems and are also useful for winter maintenance vehicles in which knowledge of the friction coefficient can be used to determine the amount and type of deicing chemicals to be applied to a winter roadway.

Chapter 1: Introduction to Vehicle-Based Friction Measurement

1.1 Background

The forces generated by the tires are very crucial for vehicle dynamics and controls because they are the only force sources that a vehicle has from the ground. The maximum forces that tires can supply are determined by the maximum value of the tire-road friction coefficient for a given normal vertical load on the tire.

Many vehicle control systems, especially active safety control systems such as adaptive cruise control (ACC), ABS, traction control, collision warning/avoidance control, four-wheel-steering, and stability control system can greatly profit from being made "road-adaptive," i.e., the control algorithms can be modified to account for the external driving condition of the vehicles if the actual tire-road friction coefficient is available in real time. For example, in the ACC system, the road condition information from friction coefficient estimation can be used to adjust the spacing headway that the ACC vehicles should maintain.

The identification of tire-road friction coefficient is also useful for winter maintenance vehicles like snowplows. In the case of such vehicles, which have to operate in a harsh winter road environment, the knowledge of friction coefficient can help to improve the safety of operation. Further, the vehicle operator can use this information to adjust the amount and kind of deicing material to be applied to the roadway. It can also be used to automate the application of deicing material.

1.2 Review of Results on Tire-Road Friction Coefficient Estimation

For a given tire, the normalized traction force, m, is defined as:

$$m := \frac{\sqrt{F_x^2 + F_y^2}}{F_z} \tag{1.1}$$

where F_x, F_y, and F_z are the longitudinal, lateral, and normal forces acting on the tire. If we consider only longitudinal motion, and then lateral force F_y can be neglected, which gives:

$$m := \frac{F_x}{F_z} \tag{1.2}$$

The objective of friction coefficient estimation system is to predict the limit of force that the tire can provide, or the maximum friction coefficient, m_m, for different road surfaces.

Recently, the tire-road friction coefficient estimation has become an intensive research area and many different approaches have been studied in literature and demonstrated experimentally [1, 2, 3, 6, 7, 8, 9, 10].

U. Eichhorn et al. proposed an acoustic approach in which a microphone is mounted on the car to “listen” to the tire, and the sound that the tire makes is used to infer the friction coefficient [1, 2]. An analysis and experimental results show that the tire noise not only correlates to both the friction demand and tire tread deformation, but also correlates to the parameters that affect the friction coefficient such as road type and presence of water. However, the complex nature of the sources of the tire noise makes it difficult to estimate friction coefficient accurately and reliably [2].

Eichhorn and Roth [1] and Uno and Sakai et al. [3] investigated another approach using optical sensors installed at the front bump of the car to estimate the road surface types and possible lubricants based on the information from the ground reflections. The advantage of this optical approach is that it is able to preview the road friction information before the vehicle reaches that point in the road. However, there are

considerable difficulties in maintaining the sensors clean and reliable under different light and weather conditions.

In [1,2], the authors also discussed another friction estimation method using strain sensors vulcanized into a kevlar-belted tire (to avoid signal distortion from a steel belt) tread to measure the *x*, *y*, and *z* deformations of the tread as a function of its position in the road-tire contact patch. These deformations are the direct results of the longitudinal, lateral, and normal forces applied to the contact patch and therefore contain enough information about the magnitude of these forces and relationships among them to estimate the friction coefficient. While fairly promising this approach requires the development of a sophisticated instrumented tire with embedded sensors.

The desire of avoiding additional sensors and/or instruments makes another class of friction coefficient estimation approaches—slip-based methods more attractive because they just use the standard sensors already on-board an intelligent vehicle.

Tire slip occurs whenever pneumatic tires transmit forces. According to the definition in SAE670e [4], the longitudinal slip is defined as the relative difference between a driven wheel's circumferential velocity and the vehicle's absolute velocity v as follows:

$$s_x = \frac{w r_e - v}{\max(v, w r_e)} \tag{1.3}$$

where w is the wheel speed of revolution and r_e is the effective tire radius. Notice this definition is more suitable for braking case, where the slip will be –1 (-100%) when the wheel locks up. For acceleration, the denominator of the slip calculation equation will be changed to be the wheel speed instead of the vehicle absolute velocity, therefore, the slip is 1 (100%) when the wheel spins at zero velocity.

The normalized force (or friction coefficient) generated at a tire is a function of the amount of the slip at that tire. The most famous model that describes this relationship is the so-called "Magic Formula" tire model developed by Pacejka [5], which is plot in Figure 1.1 for different road surfaces. Here, the vertical force, F_z, is assumed to be a

constant. As can be seen from the figure, for different road surfaces, the forces generated by tire vary significantly. Near the origin, the normalized force increases with increasing slip until a critical slip value, where the force reaches its maximum value and then starts to decrease slowly.

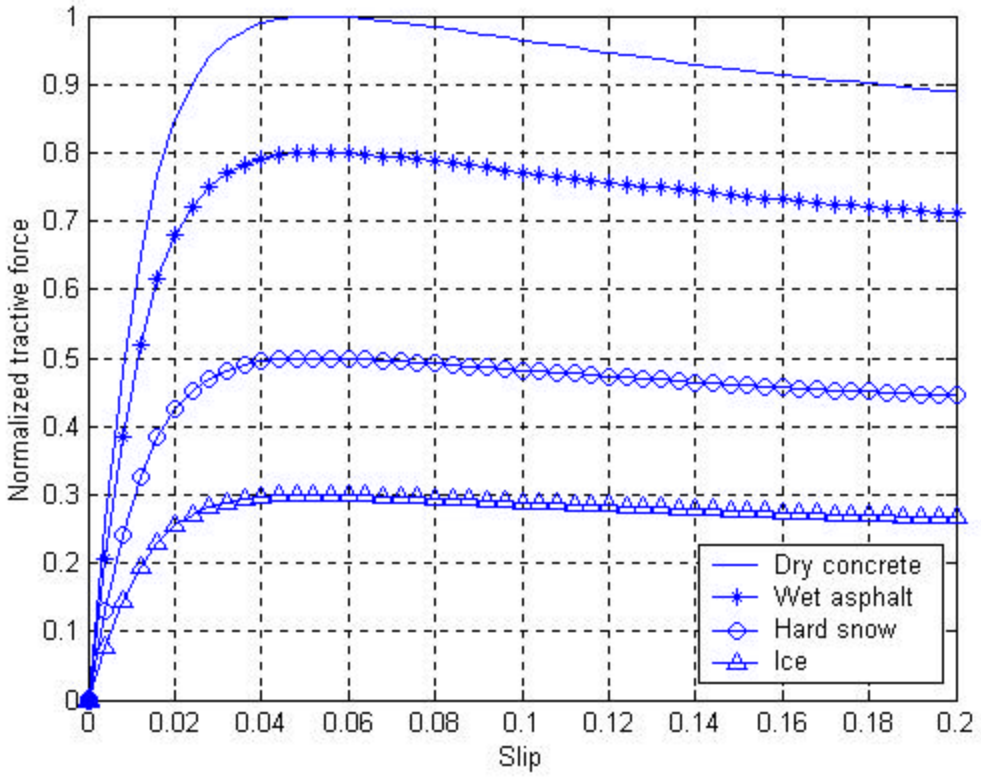

Figure 1.1: Typical normalized traction force vs. slip for different road surfaces

The basic idea of the slip-based friction coefficient estimation is to use the data collected in the low-slip region, or the linear part of the slip curve near the origin, to estimate the linear relationship between measured tire force and slip, the slip-slope. And then map the estimated slip-slope to the maximum friction coefficient m_m of the corresponding surface by using a classifying function, which is designed based on experimental experience.

Recently, the slip-slope based friction coefficient estimation approach for acceleration (traction) situation has been extensively investigated and successfully demonstrated to be able to differentiate the frictions of different road surfaces for a limited set of operating conditions [6, 7, 8, 9].

Gustafsson first proposed the slip-slope based friction coefficient estimation method in [6] where a Kalman filter is designed to estimate slip-slope of the friction-slip curves and map the slopes to friction coefficients based on test data in the low-slip regions. The system works in acceleration (traction) on a front wheel drive passenger car, with the rear wheel ABS sensor providing the absolute velocity reference and front wheels serving as the slipping wheels. The traction contribution of rear wheels are assumed to be zero. The slip is calculated directly from the difference between the speed of front wheels and rear wheels. The normalized traction force, m, is calculated from the estimated engine torque (based on measured injection time and engine speed) and the normal force. The Kalman filter recursively calculates the slip-slope during acceleration. Extensive testing on icy, snowy, gravel, wet, and dry surfaces with four different types of tires indicates that the estimated slip-slope could be used to classify the friction levels of different road surfaces.

Yi et al. [7] and Hwang and Song [8] also provide more experimental evidence that the slip-slope could be used to classify the road surface during normal acceleration. Both Yi and Hwan employ friction estimation methods during regular traction that are quite similar to Gustafsson's. Yi et al. used an observer to estimate the drive shaft axle torque, and the results show a difference between the slopes of slip curves on wet and dry concrete surfaces. The results from Hwang and Song indicate that the slip-slope in the linear part of the normalized traction force vs. slip curve is significantly larger for a dry asphalt surface than that of an artificial ABS test slippery surface.

However, the common disadvantages for the approaches described above are they need to use the driven wheel speed as an estimate of the absolute speed. This will not be accurate for an all-wheel drive vehicle and/or during braking (in which all wheels will slip and contribute forces). Besides, the systems can work only in low-slip (linear part) regions during accelerations in order to accurately estimate the slip-slopes. These limitations considerably restrict the applicable scope for these systems.

In 2001, Müller and Uchanski [9] broadened the slip-slope friction coefficient estimation to braking situations. A brake pressure sensor is employed to determine the brake torque of an individual wheel, which are used to calculate the tire forces. The rear wheel brakes of the experimental vehicle are turned off and served as the absolute velocity reference. So, only the front wheels are considered as the source of the braking force. However, in practice, a brake pressure sensor is too expensive to implement and all of the wheels would contribute forces, which make this approach difficult to be applied in real life.

Besides the longitudinal slip approaches, Hahn et al. [10] proposed a lateral dynamics approach to estimate the friction coefficient using the slip angle calculated from differential GPS information.

In summary, the previously suggested approaches about the longitudinal slip-based friction coefficient estimation can work for either front-wheel drive acceleration or front-wheel braking situations (the situation where only the tires on one axle of the vehicle contribute forces), respectively. However, in the reality, there are many cases where all the tires on both front and rear axle of the vehicle contribute forces such as all-wheel drive vehicle and regular braking.

1.3 Project Contributions

This project concentrates on the development of a new slip-based friction coefficient identification approach, which can accommodate both front/rear-wheel drive and all-wheel drive vehicle acceleration and braking situations, and therefore greatly expand the applicable scope for the friction coefficient identification. Besides, the estimation system can work in both low-slip region (linear part) and high-slip region (nonlinear part) as well. Moreover, the use of GPS makes the slip calculation more accurate and available under all the operational conditions. In addition, several practical implementation issues such as signal impulsive noise and bias are well addressed using several novel filters.

1.4 Overall Project Objectives

The primary tasks involved in this project are:

- Develop a unified friction coefficient estimation approach, which can accommodate both acceleration (traction) and braking situations for both rear/front-wheel drive and all-wheel drive vehicles.
- Design a real-time estimation algorithm based on the proposed approach, which ensures high immunity to noise and fast tracking ability.
- Demonstrate the experimental performance of the developed friction coefficient estimation system on SAFEPLOW for different road surfaces. The SAFEPLOW is an instrumented winter highway maintenance vehicle and will be described in the later chapters.

The rest of the project is organized in the following way. In Chapter 2, vehicle dynamic models and tire models are studied. In Chapter 3, a Recursive Least Square identification algorithm combined with change detection strategy is developed. Experimental implementation of the developed identification system on the SAFEPLOW is described in chapters 4 and 5. The experimental system hardware and software are described in chapter 4. Detailed experimental results are presented in chapter 5. Finally, conclusions are presented in chapter 6.

Chapter 2: Vehicle Dynamics and Tire Model

2.1 Introduction

In order to estimate the road-tire friction coefficient using slip-based approach, we need to know both the slip and the force (traction or braking force) generated by the tire. The slip can be easily calculated according to the Eq. 1.3 if both absolute vehicle speed and wheel speed can be reliably measured. For the tire force, basically, there are two possible procedures to obtain the force. The first method is to compute the complete engine, powertrain, drive shaft axle, and wheel dynamics, and then calculate the traction force based on those measured data as employed by Yi et al. in [7]. However, to implement this method, a detailed knowledge of the engine characteristics and the transmission rate of different gears and associated measurements such as pedal position, engine speed and transmission gear position are necessary. Even more, if we consider the braking case, the knowledge about the brake system dynamics and the actual brake effort distribution rate between front and rear tires is required, which is usually difficult to obtain.

The second approach is based on the vehicle longitudinal dynamics and calculates the total longitudinal force rather than individual tire force by just using an accelerometer to measure the vehicle's acceleration/deceleration. However, since the slip is measured responding to individual tires, the measured total force has to be divided between the front and rear tires with respect to the driving wheels and the brake effort distribution ratio as described in [11]. But the brake effort distribution ratio is difficult to measure and it may vary during braking.

In this chapter, a novel method that just uses the measured total longitudinal force from an accelerometer and avoids dividing it between the front and rear tires is developed for both traction and braking situations. The proposed method is applicable for front-wheel drive, rear-wheel drive, and all-wheel drive vehicles.

2.2 Vehicle Longitudinal Dynamics

A dynamic model of the vehicle longitudinal motion can be obtained by applying Newton's laws. The vehicle longitudinal position is measured along its longitudinal axis.

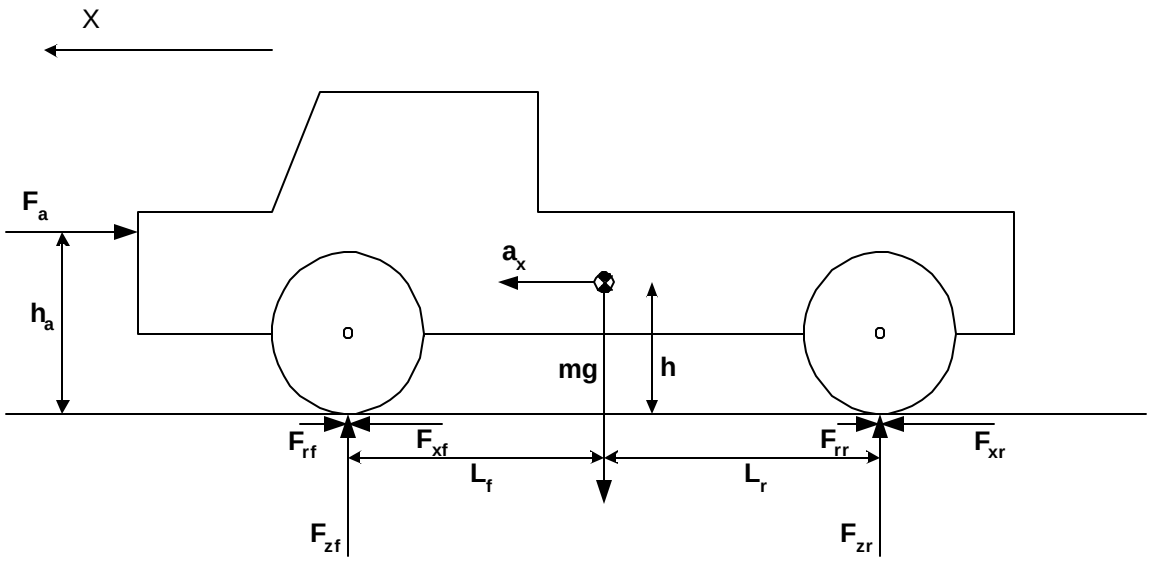

Figure 2.1 Vehicle longitudinal dynamics schematic diagram

Consider a bicycle type model (the difference between right and left tires is ignored) shown in Figure 2.1, ignoring the road gradient and wind speed, the longitudinal dynamics can be represented as:

$$ma_x = F_{xf} + F_{xr} - F_r - D_a V^2 \tag{2.1}$$

where,

m is the total mass of the vehicle.

a_x is the longitudinal acceleration/deceleration.

F_{xf} and F_{xr} are the front and rear wheel traction/braking forces.

$F_r = F_{rf} + F_{rr} = C_{roll} mg$ is the rolling resistance force with C_{roll} being the rolling resistance coefficient.

$D_a = \frac{1}{2} \rho C_d A$ is the aerodynamic drag force with ρ being the air density, V the longitudinal velocity, C_d the aerodynamic drag coefficient, and A the frontal area of the vehicle.

L_f is the distance from c.g. to the front axle; L_r is the distance from c.g. to the rear axle. $L = L_f + L_r$ is the wheelbase of the vehicle.

The total longitudinal tire force F_x therefore can be calculated as follows:

$$F_x = F_{xf} + F_{xr} = m|a_x| + |F_r| + |D_a V^2|, \qquad \text{if } a_x \geq 0 \text{ or acceleration}$$

$$F_x = F_{xf} + F_{xr} = m|a_x| - |F_r| - |D_a V^2|, \qquad \text{if } a_x < 0 \text{ or deceleration} \tag{2.2}$$

Thus, once the vehicle longitudinal acceleration/deceleration, a_x, is measured by using an accelerometer and corrected for bias, the total vehicle longitudinal force, F_x, can be obtained based on Eq. (2.2).

2.3 Determination of the Normal Force

As the definition of friction coefficient (Eq. 1.2) indicates, the normal force plays an important role in determining the amount of the force the tire can possibly generate. For the same road surface and tire, the bigger the normal force, the bigger the longitudinal force could be. The mass of the vehicle contributes the major part of the normal forces on the tires, and the other forces acting on the vehicle redistribute the normal forces between the tires. If the vehicle is traveling in a straight line on level road, the normal forces at the front and rear tires can be calculated using a static force model of the vehicle as described in [12]:

$$F_{zf} = \frac{mgL_r - ma_x h - D_a V^2 h_a}{L}$$

$$F_{zr} = \frac{mgL_f + ma_x h + D_a V^2 h_a}{L} \tag{2.3}$$

During cornering, the normal forces of the right and left tires on both front and rear axle are different due to vehicle roll moment. However, since we are using a bicycle model, the total normal forces for the front and rear axles will not change.

The normal force calculation method described above is based on the static force model ignoring the influence of the vibration of the suspension. This method gives a fairly reasonable estimate of the normal force, especially when the road surface is fairly paved and not bumpy. However, if the road surface is very bumpy, a dynamic normal force estimation method incorporating the suspension dynamics will provide more accurate normal force. Such a method was proposed by Hahn and Rajamani in [10]. A two degree-of-freedom quarter-car model of an automotive suspension is shown in Figure 2.2. The sprung mass m_s is the mass of the vehicle body, the unsprung mass m_u is the mass of the tire and axle. k and b are the stiffness and damping of the suspension and k_t and b_t are the stiffness and damping of the tire.

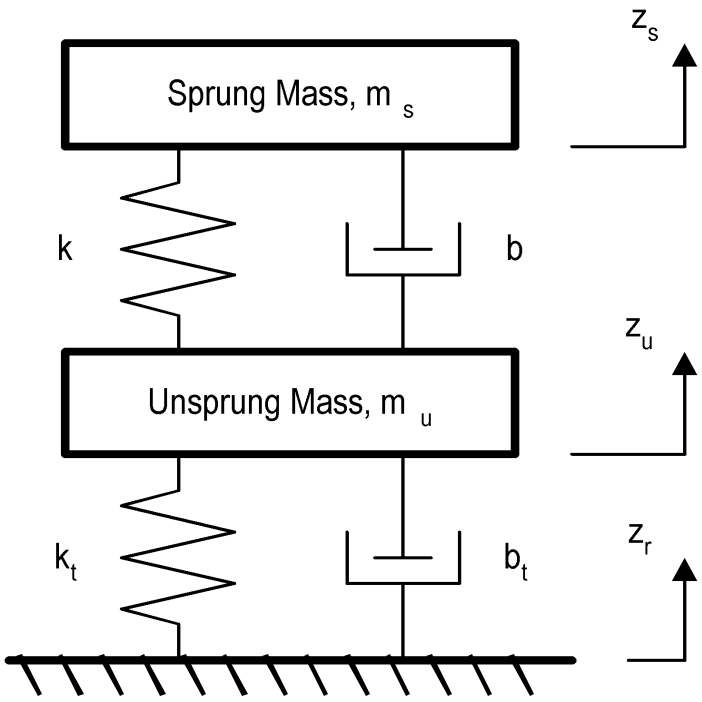

Figure 2.2 Schematic diagram of an automotive suspension

The equation of motion for the unsprung mass can be written as:

$$m_u \ddot{z}_u = -b_t(\dot{z}_u - \dot{z}_r) - k_t(z_u - z_r) + b(\dot{z}_s - \dot{z}_u) + k(z_s - z_u) \qquad (2.4)$$

Thus the normal force acting on the tire can be estimated by measuring $\ddot{z}_u$, $z_s - z_u$, $\dot{z}_s - \dot{z}_u$ and then using the following equation:

$$F_z = b_t(\dot{z}_u - \dot{z}_r) + k_t(z_u - z_r) = b(\dot{z}_s - \dot{z}_u) + k(z_s - z_u) - m_u\ddot{z}_u \quad (2.5)$$

This normal force estimation method calculates the normal force dynamically using the dynamic relations at each wheel. It is supposed to be more accurate. However, in practice, it would be expensive to measure the suspension deflection, $z_s - z_u$, and relative suspension velocity, $\dot{z}_s - \dot{z}_u$. Besides, for heavy-vehicle equipped with steel leaf spring suspensions, both the composite vertical stiffness and damping are nonlinear functions of load and deflection [13], which make this method even more difficult to implement in our test SAFEPLOW.

2.4 Tire Model

The longitudinal force (traction/braking) generated at each tire is known to depend on the longitudinal slip, the tire-road friction coefficient, and the normal force applied at the tire. The "Magic Formula" tire model developed by Pacejka et al. [5] is generally accepted as the most accurate model in describing the relationship between tire slip and force. The model was developed using the data from single tire experiments, all conducted on a dry asphalt road surface. The model for the longitudinal force is as follows:

$$F_x = D\sin\{C\arctan[Bs_x - E(Bs_x - \arctan(Bs_x))]\} \quad (2.6)$$

where,

F_x is the longitudinal force generated by individual tire,

s_x is the longitudinal tire slip,

$C = a_0$ is the shape factor,

$D = a_1F_z^2 + a_2F_z$ is the peak factor,

$B = \dfrac{(a_3F_z^2 + a_4F_z)e^{-a_5F_z}}{a_0(a_1F_z^2 + a_2F_z)}$ is the tire stiffness factor,

$E = a_6F_z^2 + a_7F_z + a_8$ is the curvature factor,

F_z is the tire normal force.

$a_{1,\ldots,8}$ are the coefficients determined through experimentation

Figure 2.3 shows the traction and braking forces vs. slip relationships for a variety of road surfaces computed using the above Magic Formula model with some values for a_1-a_8. As it indicates, $m = \frac{F_x}{F_x}$ is an increasing function of slip s until a critical slip value, where m reaches $m_{\max}$ and starts decreasing slowly.

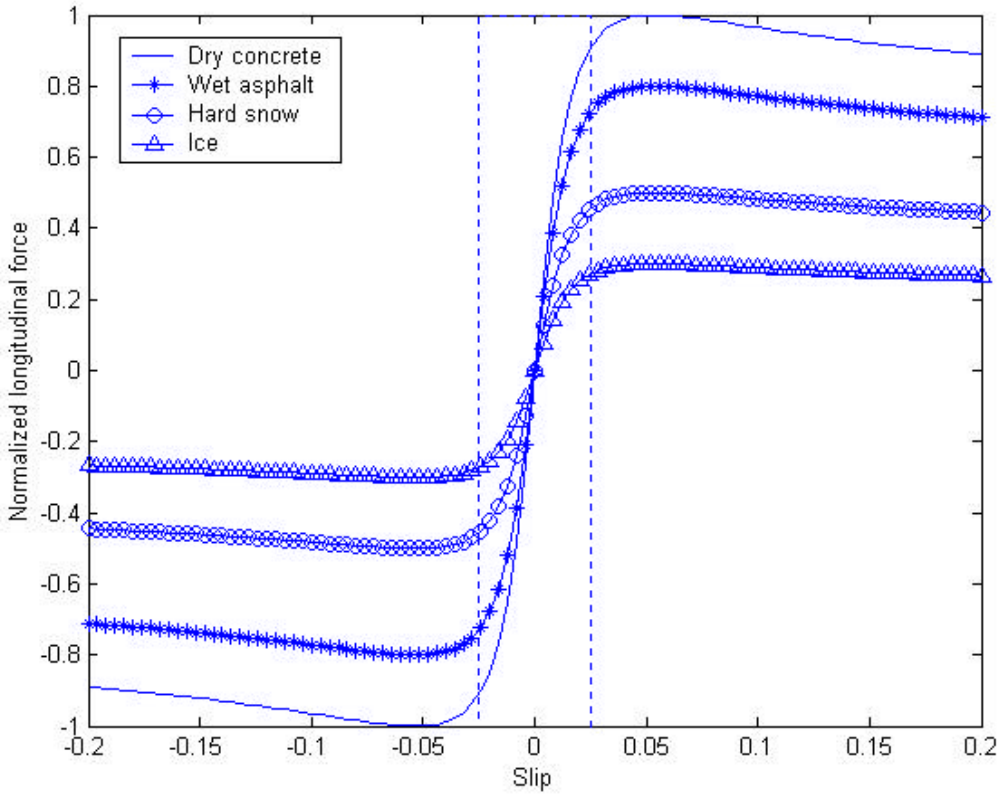

Figure 2.3 Longitudinal force vs. slip computed using Magic Formula model

Notice that in order to use the Magic Formula model for a particular tire, one needs to find out all the eight parameters a_1 to a_8 experimentally by fitting the measured testing data of that particular tire on various normal forces and longitudinal slips to the formulae. It would be very difficult to estimate the eight parameters in real-time, which makes it hard to utilize this model to identify the road surface friction coefficient. However, the

Magic Formula model does provide basis for the slip-slope based friction coefficient identification method. In the model, the coefficient D represents the peak value of the friction curve. Its value greatly dependents on the road surface and changes significantly from dry asphalt/concrete to snow/ice. The value of the shape factor C also changes from surface to surface with higher value on asphalt and lower value on snow. The slope of the curve at the origin (slip=0) is called slip-slope or stiffness, which is equal to the product BCD. Where the stiffness factor B is primarily determined by the tire properties and independent of the changes in road surface. Therefore, the change of the slip-slope BCD caused by the variations of C and D could be used to indicate the change in road surface characteristics, as shown in the dotted line block in Figure 2.3.

2.5 Friction Coefficient Estimation for Both Traction and Braking

This section develops a unified slip-slope based friction coefficient estimation method for front/rear-wheel drive and all-wheel drive vehicles in both traction and braking situations without the knowledge of traction/braking force distribution ratio between front and rear axles.

As described in the previous section, the longitudinal force generated at an individual tire is proportional to its longitudinal slip in the low-slip region or the linear part of the friction curve for given road surface and normal force. This relationship can be described as:

$$m = \frac{F_x}{F_z} = Ks_x \tag{2.7}$$

where K is the slip-slope, whose value changes with road surface conditions and could be used to predict the maximum value of the friction coefficient (or the normalized longitudinal force), m_m. However, the above equation holds only for individual tire, which means that the longitudinal force F_x, normal force F_z, and the slip s_x in the equation have to be the values for the same single tire. For the longitudinal vehicle

bicycle model, we can consider the right and left tires together, but there are still two (front and rear) tires that will contribute longitudinal force during all-wheel driving and braking. Thus, in order to apply the slip-slope estimation method, the forces and slips for the front and rear tires need to be calculated respectively.

The normal forces for the front and rear tires can be easily calculated if the static normal force model described in section 2.3 is used. However, the longitudinal forces of the front and rear tires are difficult to measure individually. Previous researchers who implemented the slip-slope method dealt with this problem in the following ways:

- Estimate the slip-slope just for traction (acceleration) situation on a front-wheel drive car in which the rear tire longitudinal force can be ignored as described in [6, 7]. However, it would be difficult to extend this method to work in braking situations as well as in all-wheel drive acceleration in which both front and rear tires contribute the longitudinal force.

- Estimate the friction coefficient for braking situation by using a brake pressure sensor to measure individual tire braking force as described in [9] or by using a brake effort distribution ratio to dividing the measured total braking force into front and rear two parts as described in [11]. However, the brake pressure sensor is expensive to implement in practice and the brake effort distribution ratio may vary during braking.

- Estimate the tire slip from the difference between driving and driven wheels. As described in [6, 7], rear wheel speed is served as absolute vehicle speed during acceleration for a front-wheel drive car. And in [9], the rear wheel brake is turned off during braking to provide the absolute speed reference. However, for normal vehicle braking and all-wheel drive vehicle acceleration situations, these methods would not be able to provide the absolute speed.

For an all-wheel drive vehicle, the linear relationships between slip and normalized longitudinal force for the front and rear tires can be written as:

$$\mu_f = \frac{F_{x_f}}{F_{z_f}} = K_f s_{x_f} \tag{2.8}$$

$$\mu_r = \frac{F_{xr}}{F_{zr}} = K_r s_{xr} \tag{2.9}$$

$$F_x = F_{xf} + F_{xr} \tag{2.10}$$

where, F_x is the vehicle total longitudinal force, which can be calculated as described in section 2.2. K_f and K_r are the slip-slopes of the front and rear tires whose values are determined by the front and rear tire properties and road surface characteristics. Combining the above three equations, we can get:

$$F_x = F_{xf} + F_{xr} = K_f F_{zf} s_{xf} + K_r F_{zr} s_{xr} \tag{2.11}$$

If we assume that the front and rear tires are on the same road surface condition, which is true for most driving situations, then the difference between the values of K_f and K_r is mainly dominated by the tire properties (including the tire type and number of tires for front and rear axles), which are independent of the road surface condition. Therefore, K_f and K_r can be related as:

$$K_f = \alpha K_r \tag{2.12}$$

where, α is a ratio coefficient determined by the front and rear tire properties and independent of road surface condition. Thus, the relationship between total force and slips can be written as:

$$F_x = F_{xf} + F_{xr} = K_f F_{zf} s_{xf} + K_r F_{zr} s_{xr} = K_r (\alpha F_{zf} s_{xf} + F_{zr} s_{xr}) \tag{2.13}$$

where, $F_x, F_{zf}, F_{zr}, s_{xf}, s_{xr}$ can be measured or calculated in real-time, and α can be determined experimentally for particular vehicle. For example, if the vehicle chassis

configuration is as shown in Figure 2.4, with two tires on the front axle and four tires on the rear axle (which is the configuration of the SAFEPLOW used in this project), and all tires are exactly same, then $a = 1/2$. If the front tires are different from the rear tires in terms of wear level and tread pattern, then the value of a could be experimentally determined as some value less than 0.5. But, its value will stay constant for a considerably long time once it is determined and will not change with road surface friction coefficient. Adaptation for a can potentially be used also.

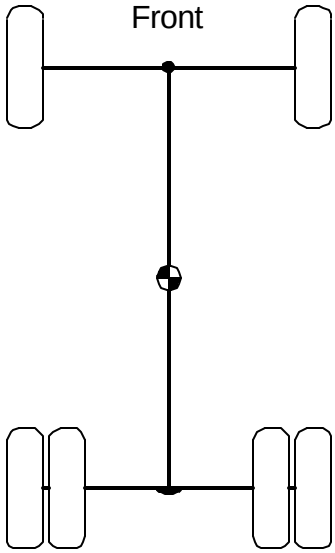

Figure 2.4 Chassis tire configuration example

If the vehicle is rear-wheel drive instead of all-wheel drive, then $a = 0$ during acceleration with ignoring the traction force of front tire and choose a as the specific value determined by the chassis configuration during braking. If the vehicle is front-wheel drive, the equations for K_f can be derived similarly as:

$$F_x = F_{xf} + F_{xr} = K_f F_{zf} s_{xf} + K_r F_{zr} s_{xr} = K_f (F_{zf} s_{xf} + \frac{1}{a} F_{zr} s_{xr}) \qquad (2.14)$$

where, $\frac{1}{a} = 0$ or $a = \infty$ during acceleration and a is the specific value determined by the chassis configuration during braking.

Since the SAFEPLOW used in this project is a rear-wheel drive vehicle, we present the rear-wheel drive case for the friction coefficient identification in the estimation algorithm derivation in the following chapter. However, the same algorithm can also be used for front-wheel drive and all-wheel drive vehicle.

The equation (2.13) can be rewritten as a standard parameter identification format as:

$$y(t) = j^T(t)q(t) \tag{2.15}$$

where, $y(t) = F_x$ is the system output, $q(t) = K_r$ is the unknown parameter, and $j(t) = aF_{zf}s_{xf} + F_{zr}s_{xr}$ is the measured regression vector. The only unknown parameter K_r can be easily identified in real-time using standard parameter identification approaches as will be addressed in the next chapter. Once the slip-slope K_r is identified, it can be connected with the road surface condition or the maximum friction coefficient by a classification function.

Since the above method incorporates both front and rear tire forces and slips, it can be used to identify the friction coefficient for traction and braking situations on rear/front-wheel drive and all-wheel drive vehicles.

Notice that the above slip-slope based approach is for low slip region (linear part of the friction-slip curves) only. If the slip is high, like hard braking situation, the tire will work outside the dotted line block in Figure 2.3, which is not a linear relationship between normalized force and slip and the slip-slope based method will fail in this region. Fortunately, in the high slip region, the differences among the normalized longitudinal forces for different road surfaces are apparent enough to classify the road surfaces. Thus,

for the high slip region, the normalized force $m = \frac{F_x}{F_z}$ is directly used to classify the road surface friction level. Similarly, it can be written as standard parameter identification form as:

$$y(t) = j^T(t)q(t) \tag{2.16}$$

with $y(t) = F_x$ as the measured longitudinal force, $q(t) = m$ as the unknown parameter, and $j^T(t) = F_z{}^T = F_z$ as the normal force.

Chapter 3: Identification Algorithm Design

3.1 Introduction

From the vehicle control systems points of view, the tire-road friction coefficient estimator has to satisfy the following desirable requirements:

- The estimated friction coefficient should be close to the actual friction coefficient with both minimal error and oscillations in steady state.
- The estimator should have the ability to track changes in the actual friction coefficient as quickly as possible (for sudden changes in road surface friction coefficient).

In this chapter, an identification algorithm using the RLS method enhanced by a Change Detection algorithm is developed. Two important filters, a peak filter and a Kalman filter, are designed to deal with signal peak noise and bias.

3.2 Identification Algorithm Design

3.2.1 Recursive Least-Squares (RLS) Identification

There are several different methods available to achieve on-line system identification, namely gradient algorithm, recursive least-squares, extended least-squares, and recursive maximum likelihood [14, 15, 16]. The recursive least-squares (RLS) algorithm was selected for this project for the following reasons:

- Fast parameter convergence rate, which allows quick adaptation under unknown and changing conditions.
- Relatively small computational effort requirement, which is crucial for real-time applications.
- High immunity to noise, which enables the RLS to maintain high quality parameter estimates.

The slip-slope model described in the previous chapter can be formulated in the parameter identification form as:

$$y(t) = j^{T}(t)q(t) + e(t) \tag{3.1}$$

where $j(t)$ is the vector of estimated parameters, $q(t)$ is the regression vector, $e(t)$ is the identification error between measured $y(t)$ and estimated value $j^{T}(t)q(t)$.

The RLS algorithm provides a method to iteratively update the unknown parameter vector, $j(t)$, at each sampling time, using the past input and output data contained within the regression vector, $q(t)$. The RLS algorithm updates the unknown parameters in the way of minimizing the sum of the squares of the modeling errors. The procedure of the RLS algorithm at each step t is as follows:

Step 1: measure the system output, $y(t)$, and calculate the regression vector $q(t)$.

Step 2: calculate the identification error, $e(t)$, which is the difference between system actual output at this sample and the predicted model output obtained from the estimated parameters in previous sample, $q(t-1)$, i.e.

$$e(t) = y(t) - j^{T}(t)q(t-1) \tag{3.2}$$

Step 3: calculate the update gain vector, $K(t)$, as

$$K(t) = \frac{P(t-1)j(t)}{l + j^{T}(t)P(t-1)j(t)} \tag{3.3}$$

and calculate the covariance matrix, $P(t)$, using

$$P(t) = \frac{1}{l}[P(t-1) - \frac{P(t-1)j(t)j^{T}(t)P(t-1)}{l + j^{T}(t)P(t-1)j(t)}] \tag{3.4}$$

Step 4: update the parameter estimate vector, $q(t)$, as

$$q(t) = q(t-1) + K(t)e(t) \tag{3.5}$$

To ensure good estimation performance, the excitation signals need to satisfy the requirement of *persistence of excitation*, which ensures that the dominant process modes are excited and enables the estimated parameters to converge to their true values. For example, a square wave input signal is a good candidate that contains sufficient frequency content to excite the dominant process modes. However, the persistence of

excitation requirement might be difficult to meet in practice. In this case, the eigenvalues of the covariance matrix will tend to become small and cause the RLS update of the estimated parameter to vary slowly, or the so-called *covariance wind-up* problem.

The parameter, l, in the above equations is called the *forgetting factor*, which is used to effectively reduce the influence of old data which may no longer be relevant to the model, and therefore prevent the covariance wind-up problem. This allows the parameter estimates to track changes in the process quickly. A typical value for l is in the interval [0.9, 1]. The size of the forgetting factor can be intuitively understood as: the RLS algorithm uses a batch of $N = \frac{2}{1-l}$ data to update the current estimation [15]. When $l = 1$, the RLS uses all the previous data from the starting time to update the current estimation. The smaller the value chosen the faster the parameters converge. However, decreasing l will increase the sensitivity of the estimation procedure to noise, which will cause the estimated parameter to become oscillatory. This brings a contradiction between fast tracking ability and high immunity to noise for the RLS algorithm, which will be addressed in the next sub-section.

3.2.2 Fast Convergence Rate and Immunity to Noise

As described before, the friction coefficient estimator is required to possess both fast convergence rate and high immunity to noise. These are, however, contradictive for the ordinary RLS algorithm. The rate of convergence is dependent on the value of forgetting factor l, which reflects the variability of the system parameters in the process.

To illustrate the influence of the size of the forgetting factor on the parameter estimation using ordinary RLS algorithm, Figure 3.1 and Figure 3.2 show the slip-slope estimation experimental results for the same process with different forgetting factors.

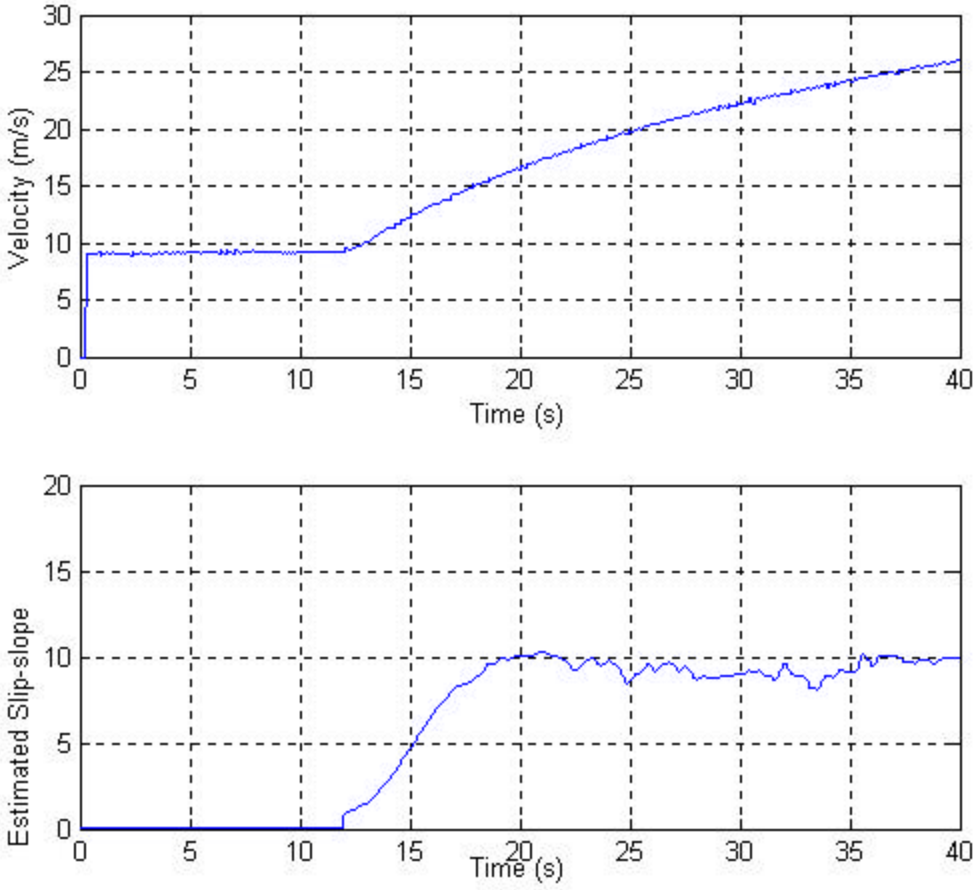

Figure 3.1: Slip-slope estimation using ordinary RLS with $l = 0.995$

In Figure 3.1, a relatively big forgetting factor is set as $l = 0.995$. As we can see, the estimated slip-slope converges about 6 seconds after the vehicle starts accelerating. It is quite slow for the friction coefficient estimation because the vehicle has traveled about 60-70 meters during the converging time without accurate estimation of tire-road friction coefficient information, which cannot satisfy the requirement 2. However, on the other hand, the estimated parameter is pretty stable and without big oscillations after it converges, which is appealing for the requirement 1.

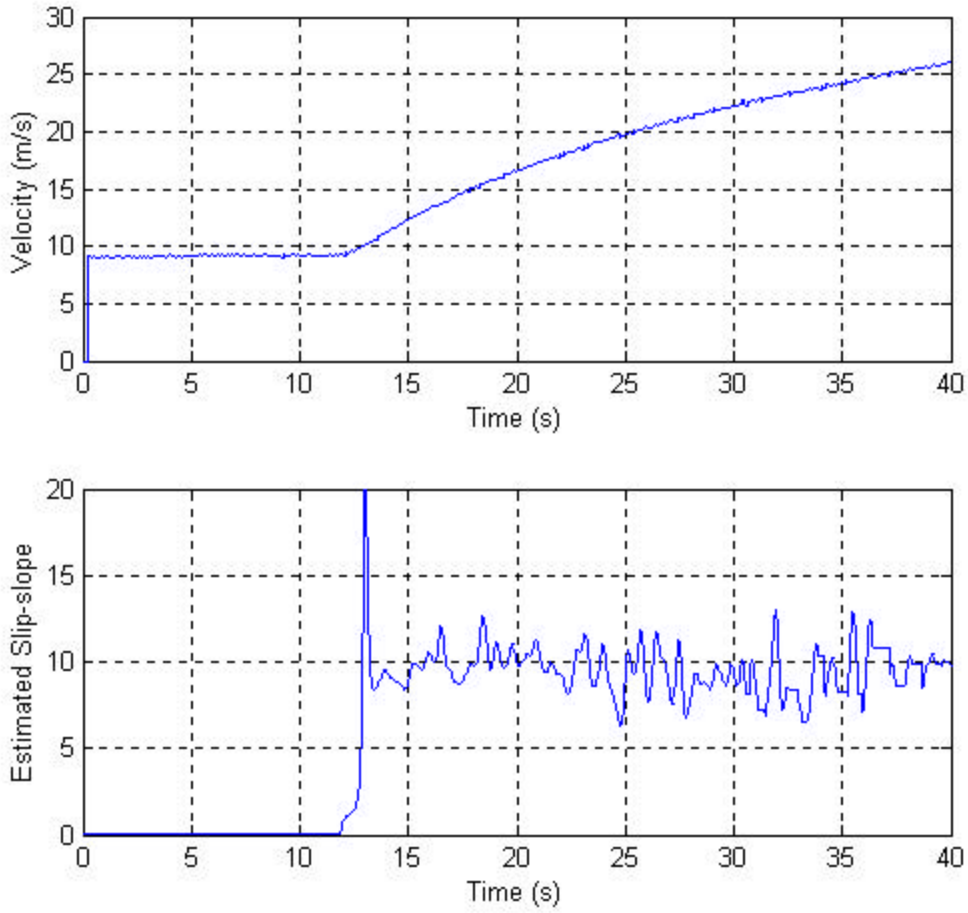

Figure 3.2: Slip-slope estimation using ordinary RLS with $l = 0.9$

On the opposite side, in Figure 3.2, a relatively small forgetting factor is set as $l = 0.9$. As we can see, the estimated slip-slope converges almost immediately (less than 1 second) after the vehicle starts accelerating. This high convergence rate makes the system more perceptive and be able to promptly respond to the sharp changes in road condition, which is very crucial and desired for vehicle control systems, especially those active safety systems. However, as shown in Figure 3.2, this high convergence rate is achieved at the expense of decreasing the system immunity to noise. The estimated slip-slope is oscillating about $\pm 35\%$ around the true value, which is not suitable for many vehicle control systems because reliable and stable friction coefficient information is necessary for them to make appropriate control decisions.

3.2.3 RLS with Gain Switching

Notice that the main reason for the convergence rate becoming slow is due to the covariance matrix (or gain matrix) becoming small. If the covariance matrix can be made adaptive to the process changes, i.e. increase the gain just during process change instants, it would allow the RLS algorithm to have high convergence rate during the process transient states and high noise immunity during the steady states.

In [15], a change detection algorithm running in parallel with a Kalman filter is used to trigger the amplification of the covariance matrix entries of the Kalman filter therefore to increase the tracking ability of the filter during transition states. Similarly, we propose an approach that combines the change detection algorithm in parallel with the ordinary RLS estimator to solve the convergence rate vs. noise immunity contradiction mentioned above.

There are several change detection algorithms available. For simplicity, the CUSUM [17] change detection algorithm is chosen to monitor the identification error $e(t) = y(t) - j^{T}(t)q(t-1)$. An alarm signal will be generated if the absolute value of identification errors have been bigger than a specific threshold value for a while. The recursive formulae of this algorithm are as follows:

$$a_t = \max(a_{t-1} + |e_t| - d, 0) \tag{3.6}$$

$$a_0 = 0 \tag{3.7}$$

The input of the change detector is the ordinary RLS identification error e_t, and the output is the alarm signal a_t.

If the output of the change detector $a_t > h$, the entries of matrix $P(t)$ will be increased by a factor to track the sudden change of friction coefficient quickly until the absolute value of the identification error drops below certain level and a_t becomes 0. Here, drift parameter *d* is used to high-pass bigger identification errors and ignore these small errors.

The threshold value h is used to determine when the alarm signal should be yield to trigger the gain amplification.

The same experimental test is used to illustrate the properties of this algorithm, as shown in Figure 3.3. A relatively big forgetting factor $l = 0.995$ is used. As it indicates, after the vehicle starts accelerating (the algorithm starts to updating), the change detector catches the great identification error and generates an alarm signal at $t = 13\text{sec}$, which triggers the gain amplification and makes the estimated slip-slope convergence to the true value almost immediately. After the estimated slip-slope converges to the true value, the identification error becomes small enough to be high-passed by the change detector, and the alarm signal disappears correspondingly. Then, the covariance matrix resumes its normal value to quell the influence of noise.

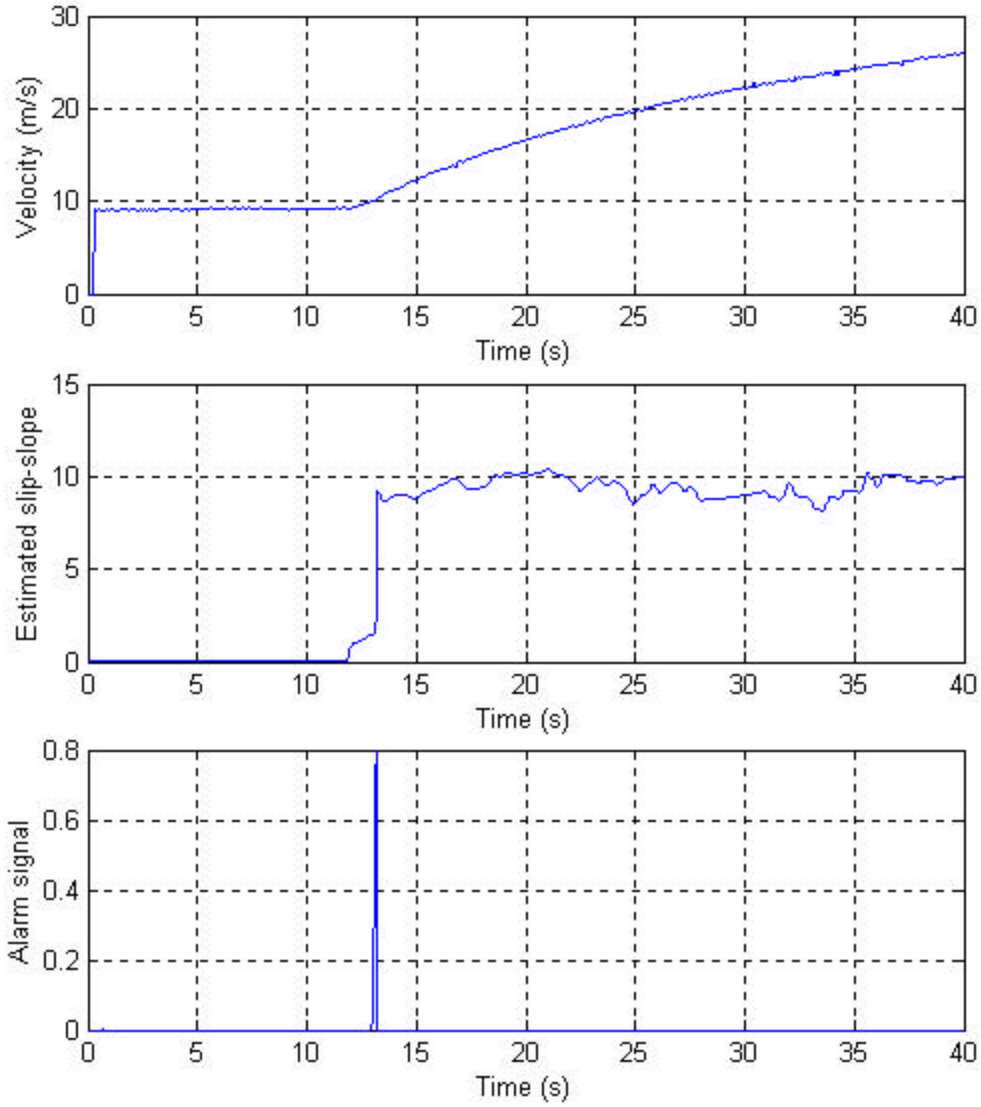

Figure 3.3: Slip-slope estimation with gain switching and $l = 0.995$

3.2.4 Updating Conditions

The precision of the estimate of the friction coefficient depends on the qualities of the estimator inputs, longitudinal force (traction/braking) and slip. If the longitudinal force or the slip is very small, the tire is working around the origin of the friction-slip curve, where the estimate will be stochastically uncertain. Besides, since the longitudinal force is calculated from the output signal of an accelerometer, if the acceleration/deceleration is

small, then the signal-to-noise ratio (SNR) of the acceleration/deceleration will be small, which may lead to overestimation of the friction coefficient. Therefore, to ensure the estimator performance, the system will stop updating the friction coefficient when the absolute value of the measured acceleration is less than 0.3 m/s^2 and the absolute value of the slip is less than 0.005. The experimental results verified that these threshold values could ensure good updates for the friction coefficient estimation.

3.3 Filter Designs

Although the RLS estimation algorithm possesses much higher immunity to noise than other estimation algorithms as mentioned in the previous section, it is still necessary to make the signals as clean as possible before sending them into the estimator in order to ensure the estimation quality. This section describes two filters designed to deal with signal peaks and bias.

3.3.1 Signal Peak Filtering

Due to environmental electromagnetic disturbances and sensor inherent defects, there are huge peaks in the wheel speed sensor signals (as shown in Figure 3.4). In order to have good parameter estimation, these peaks have to be eliminated. Otherwise, they will bring huge errors to the estimator and may cause the algorithm to fail.

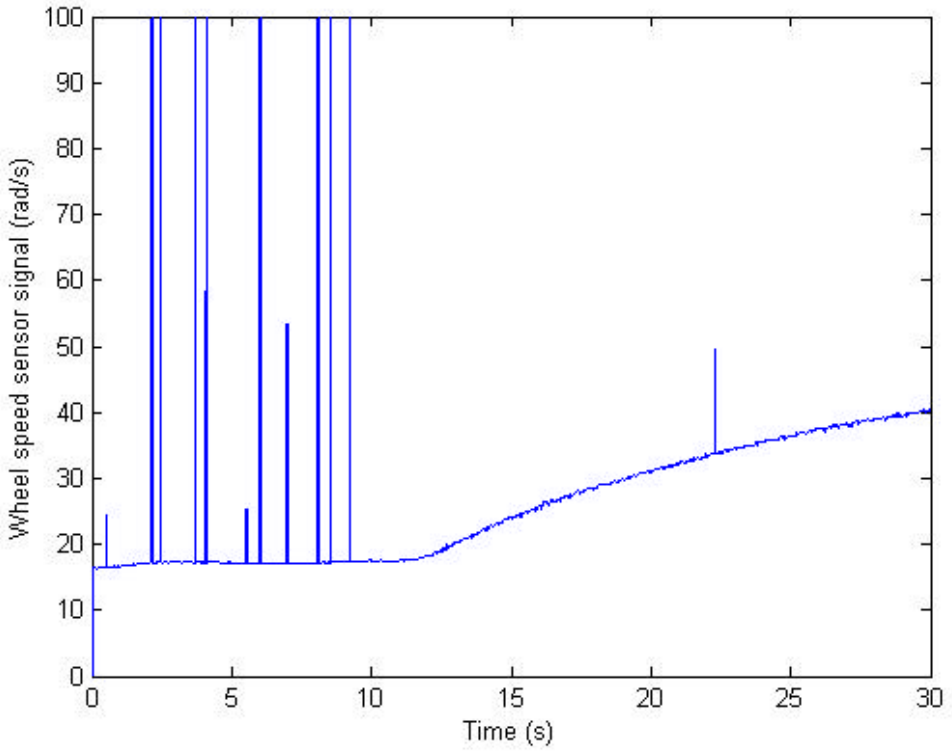

Figure 3.4 Noisy wheel speed sensor output signal

3.3.1.1 Low-Pass Filter Approach

Figure 3.5 shows the SAFEPLOW rear wheel ABS speed signal filtering result using 4-th order Elliptic low-pass digital filter with the cut-off frequency as 4Hz and the sampling rate of 200Hz. The system function of the filter is described as follows:

$$H(z) = \frac{0.00167 - 0.00269z^{-1} + 0.00367z^{-2} - 0.00269z^{-3} + 0.00167z^{-4}}{1 - 3.484z^{-1} + 4.592z^{-2} - 2.712z^{-3} + 0.605z^{-4}} \qquad (3.8)$$

Since the peaks contain extremely high frequency component, the digital low-pass filter does not work well due to aliasing. We may improve the performance of the filter by greatly increasing the sampling rate. But that will need expensive hardware requirements. Moreover, the group delay of the digital low-pass filter causes a phase lag as can also be seen from Figure 3.5.

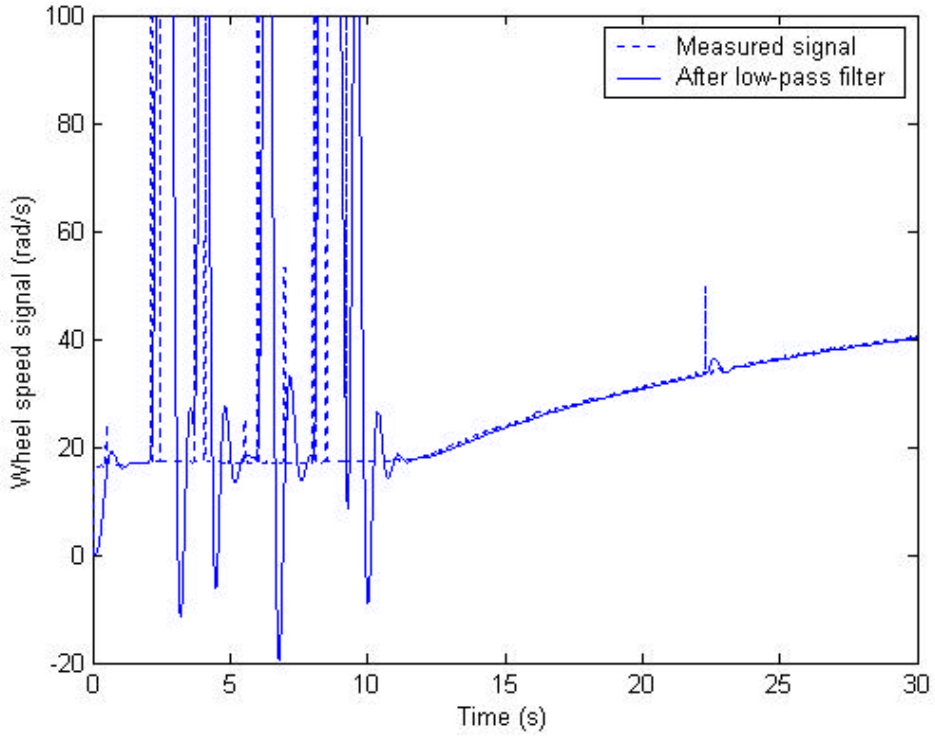

Figure 3.5 Using low-pass filter to deal with signal peaks

3.3.1.2 Median Filter Approach

Another possible approach to deal with highly noisy signal is known as running median filter, which is mostly used in image processing. The output of a $n = 2k+1$ point running median filter is the median of the previous n samples. Or, mathematically, the median filter can be described as:

$$y(n) = median[x(n-1), x(n-2), \cdots, x(n-2k-1)], \quad k = 1,2,3,\cdots \tag{3.9}$$

Median filtering can preserves sharp changes in a signal as long as these sharp changes are monotonic for at least $(n+1)/2$ samples and can completely eliminate impulsive noise that is monotonic for less than $(n+1)/2$ samples [18]. These properties are illustrated in Figure 3.6 and Figure 3.7 for a median filter of size 5, respectively. The 5-point median filter completely eliminates the sharp changes that last for less than 3 samples and preserves the sharp changes that last for at least 3 samples.

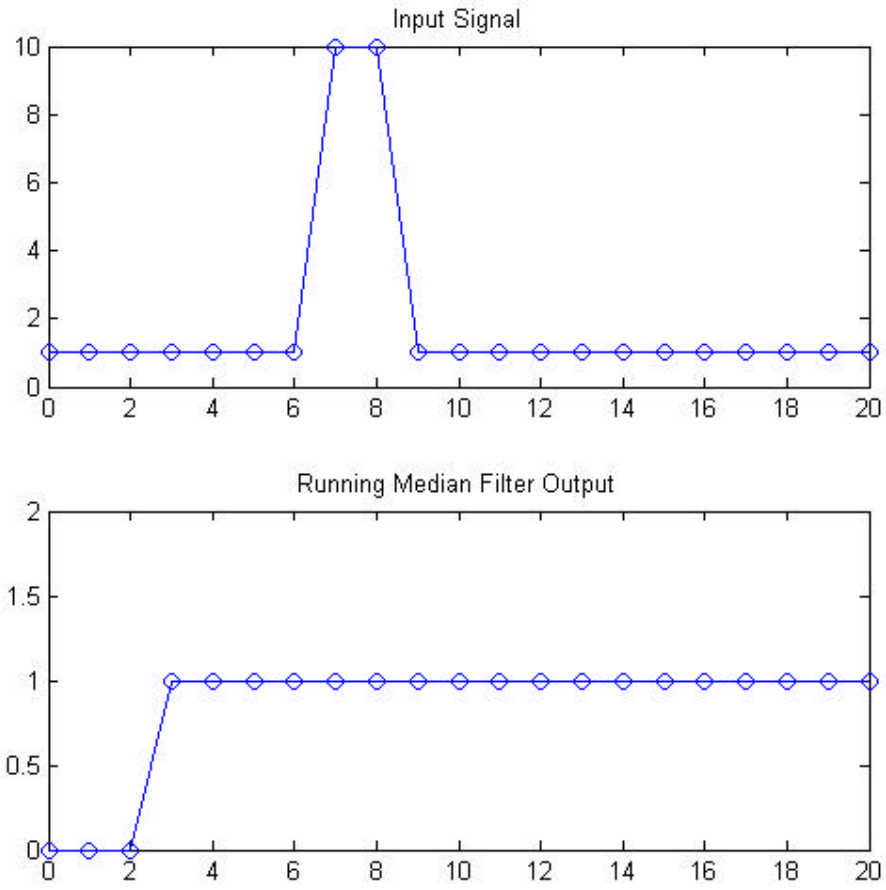

Figure 3.6 A 5-point median filter eliminates sharp changes that last for less than 3 samples

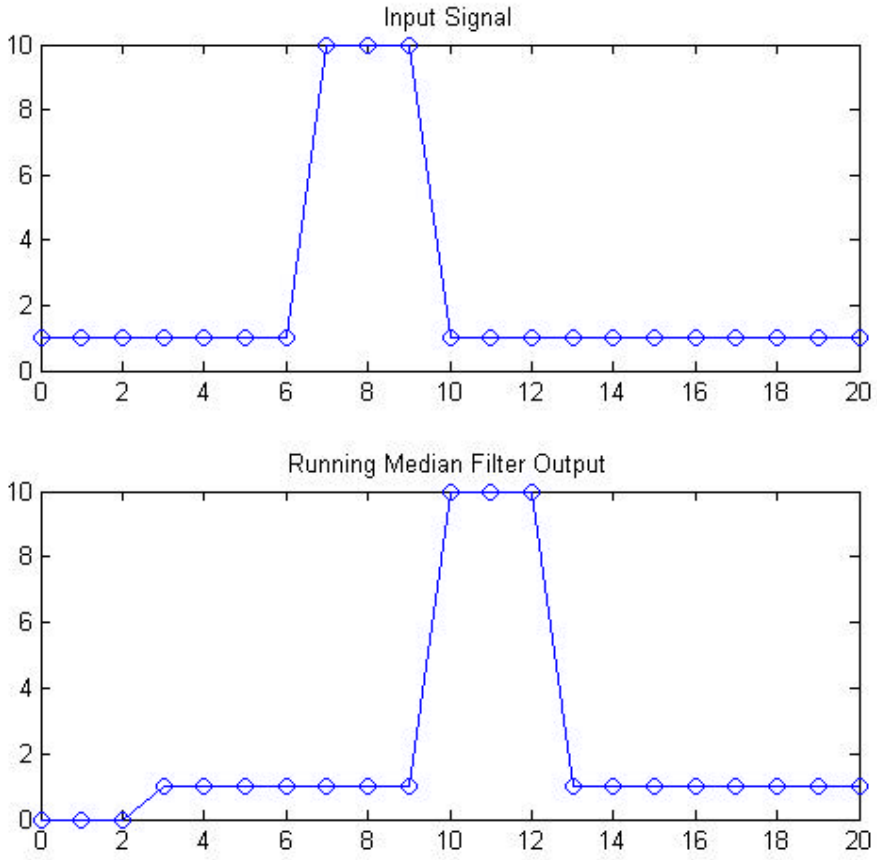

Figure 3.7 A 5-point median filter preserves sharp changes that are monotonic for 3 samples

The size of the median filter determines the width of the pulse that the filter can eliminate. To remove wider impulsive noise, bigger size median filter (more points) is needed. However, on the other hand, the density of the impulsive noise also determines the size of the median filter. To remove all the impulsive noise close to each other, we need to reduce the size of the median filter (less points). Therefore, there is a contradictory requirement about the size of the median filter. This makes it quite difficult to implement the median filter in dealing with the impulsive noise as shown in Figure 3.4, where both the widths and densities of the noise are changing with time. Figure 3.8 shows the filtering results of a 5-point median filter for the wheel speed signal. As it indicates, the median filter can eliminate most of the peaks but it fails where two peaks

are close to each other. Besides, the median filter also introduces $(n+1)/2$ samples delay.

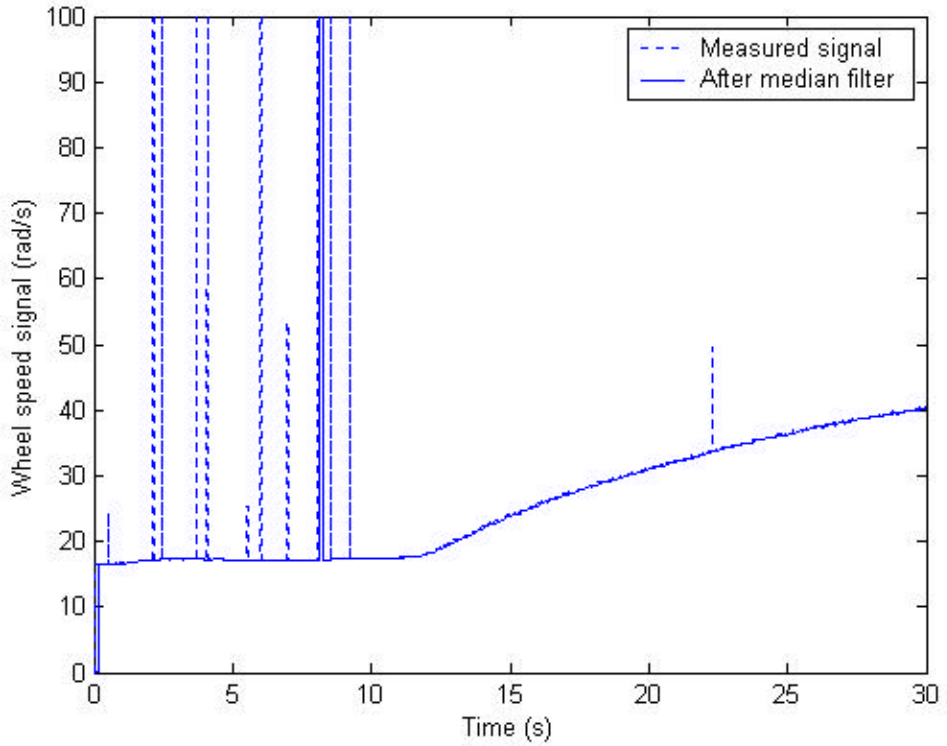

Figure 3.8 Using median filter to deal with signal peaks

3.3.1.3 Peak Filter Approach

From Figure 3.4, one can see that the impulsive noise peaks are abrupt and huge changes compared with the normal samples. A novel filter, peak filter, is designed to deal with the impulsive noise by taking advantage of these noise characteristics. The main idea of this peak filter is based on the assumption that for continuous signals, the signal magnitude difference between two adjacent samples cannot be bigger than a specific threshold value provided the sample rate is high enough. The filter can be described mathematically as follows:

$$\begin{aligned} &y(n) = x(n), && \text{if } |x(n) - z(n)| \le t, \text{ and} \\ &y(n) = y(n-1), && \text{if } |x(n) - z(n)| > t \\ &z(n) = y(n-1) \end{aligned} \tag{3.10}$$

where, t is the threshold value that determines how big the change can be allowed between to adjacent samples. Figure 3.9 shows the peak filter eliminates the undesired impulsive pulse with threshold value $t = 4$.

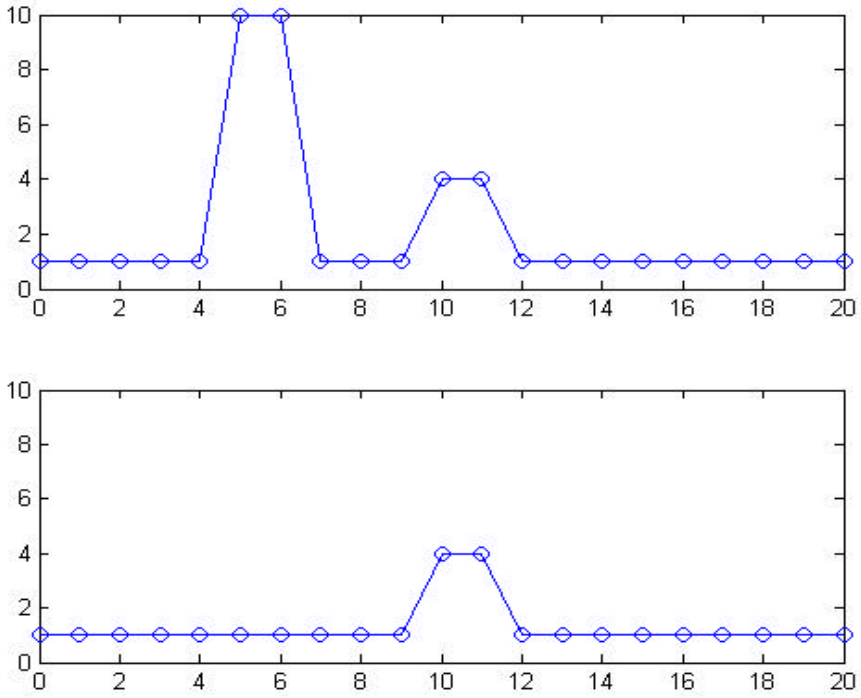

Figure 3.9 Peak filter eliminates the undesired impulsive noise

The peak filter is implemented to deal with the wheel speed impulsive noise as shown in Figure 3.10. Here, the threshold value of the peak filter is $t = 40$. As it indicates, the peak filter works pretty well in terms of completely eliminating all those peaks and without introducing any delay.

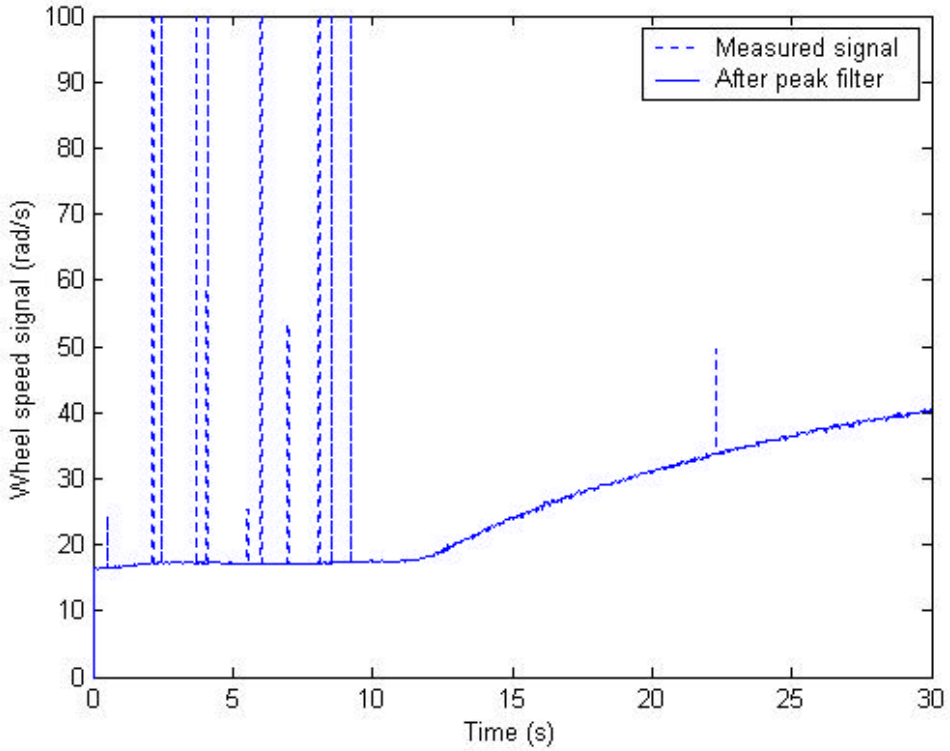

Figure 3.10 Using peak filter to deal with signal peaks

3.3.2 Estimation of Accelerometer Bias

In order to identify the friction coefficient, we not only need to accurately measure the wheel speed, but also need to estimate the forces generated at the tires. As discussed in the previous chapter, the forces are calculated mainly based on the vehicle's acceleration/deceleration. An accelerometer ADXL 105 from Analog Devices is used to measure the vehicle's acceleration/deceleration. However, there is a bias in the output signal of the accelerometer, which may change with temperature, supply voltage, and orientation of the device as well. Therefore, to calculate the acceleration/deceleration of the vehicle accurately, we need to estimate and remove the bias from the accelerometer output signal. A sensor fusion method that incorporates both accelerometer and GPS signals by a Kalman filter is used to estimate the accelerometer bias in real-time and described as follows:

Notice that the longitudinal velocity of the vehicle can be obtained from DGPS signal as:

$$V_{x\_GPS} = \dot{x} \tag{3.11}$$

The $\dot{x}$ can be obtained by numerical differentiation of the DGPS signal, which is quite accurate but very slow, usually less than 10Hz. On the other hand, the longitudinal velocity can also be obtained by integrating the measured longitudinal acceleration $\dot{V}_{x\_acc}$. Due to bias present in the acceleration signal, the velocity obtained by integration of the accelerometer output signal usually drifts. However, combination of these two signals (GPS and accelerometer) provides us a way to estimate the accelerometer bias, which is adapted from the gyro bias estimation method suggested in [19]. In the following state space system, the accelerometer measurement is used as input and the GPS signal as output. The states of the system include both the estimated longitudinal velocity, $\hat{V}_x$, and the estimated accelerometer bias, $\dot{\hat{V}}_{x\_acc\_b}$.

$$\begin{aligned}
\begin{pmatrix} \dot{\hat{V}}_x \\ \ddot{\hat{V}}_{x_acc_b} \end{pmatrix} &= \begin{pmatrix} 0 & -1 \\ 0 & 0 \end{pmatrix} \begin{pmatrix} \hat{V}_x \\ \dot{\hat{V}}_{x_acc_b} \end{pmatrix} + \begin{pmatrix} 1 \\ 0 \end{pmatrix} \dot{V}_{x_acc} + w \\
V_{x_GPS} &= \begin{pmatrix} 1 & 0 \end{pmatrix} \begin{pmatrix} \hat{V}_x \\ \dot{\hat{V}}_{x_acc_b} \end{pmatrix} + e
\end{aligned} \tag{3.12}$$

where, w and e are unknown process noise and measurement noise, respectively. For this project, the Differential GPS is used and its signal is very accurate, therefore, it is reasonable to set the measurement noise $e = 0$ in this case. But for the regular GPS, the measurement noise e could be very big due to the differentiation. The Kalman filter is applied to the above system to estimate the system states.

The time updates and measurement updates in the Kalman filter are:

$$\hat{x}_{t+1|t} = A\hat{x}_{t|t} + Bu_t \tag{3.13}$$

$$P_{t+1|t} = AP_{t|t}A^T + Q \tag{3.14}$$

$$\hat{x}_{t|t} = \hat{x}_{t|t-1} + K_t(y_t - C\hat{x}_{t|t-1}) \tag{3.15}$$

$$P_{t|t} = P_{t|t-1} - K_t C P_{t|t-1} \tag{3.16}$$

where $Q_t = Cov(w)$ is the covariance matrix of the stochastic noise w. $K_t = P_{t|t-1}C^T(CP_{t|t-1}C^T + R_t)^{-1}$ is the Kalman gain. $P_{t|t}$ is the covariance matrix for the state estimate. $A = \begin{bmatrix} 0 & -1 \\ 0 & 0 \end{bmatrix}$, $B = \begin{bmatrix} 1 & 0 \end{bmatrix}^T$, $C = \begin{bmatrix} 1 & 0 \end{bmatrix}$, and $\hat{x}_{t|t} = \begin{pmatrix} \hat{V}_x \\ \hat{V}_{x\_acc\_b} \end{pmatrix}$ is the system state.

To illustrate the performance of this approach, simulation was carried out in MATLAB/SIMULINK. In the simulation, white noise and Bias=5 was put into the accelerometer output signal. The initial value for the accelerometer bias is set as 3. The GPS signal was sampled at low frequency, 10Hz. The sampling rate for the simulation is 200Hz. In the simulation, the vehicle runs at $10\,m/s$ and starts accelerating at time 5sec with acceleration as $1\,m/s^2$. Figure 3.11 shows the inputs to the Kalman filter.

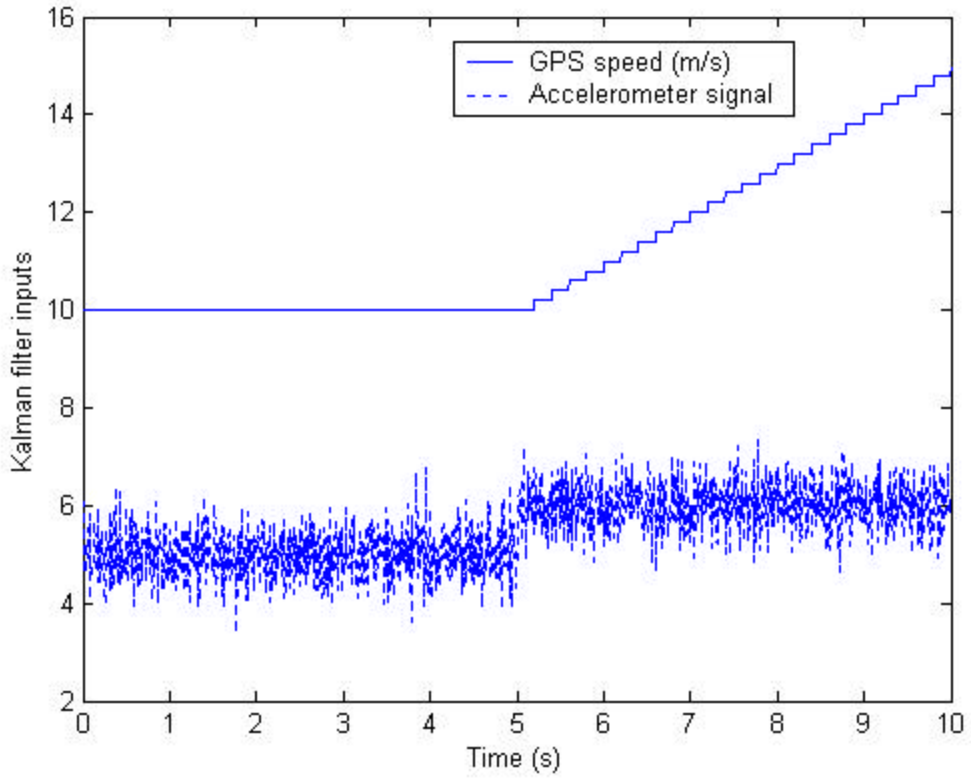

Figure 3.11 Kalman filter inputs ¾ slow GPS speed and accelerometer output

Figure 3.12 shows the outputs (estimated speed and accelerometer bias) of the Kalman filter. As one can see from the results, the Kalman filter can estimate both the vehicle speed and accelerometer bias accurately after several cycles of adaptation (less than 1 second). In the project, this Kalman filter is implemented in real-time to estimate the accelerometer bias, which is used to calculate the vehicle acceleration/deceleration.

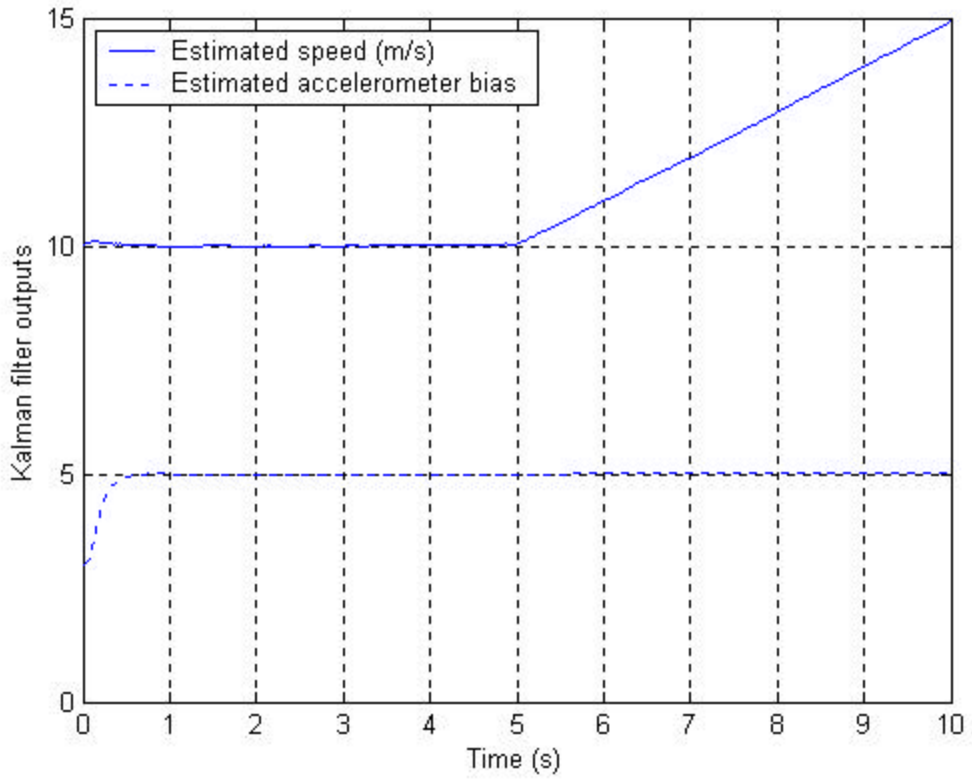

Figure 3.12 Kalman filter outputs ¾ estimated speed and accelerometer bias

Figure 3.13 shows one of the experimental results in which the SAFEPLOW performs both acceleration and deceleration. The Kalman filter is used to estimate the accelerometer bias and a 4^{th} order Elliptic digital low-pass filter is designed to attenuate the high frequency noises in the accelerometer signal. As it indicates, both the Kalman filter and low-pass filter work well in estimating the accelerometer bias and acceleration.

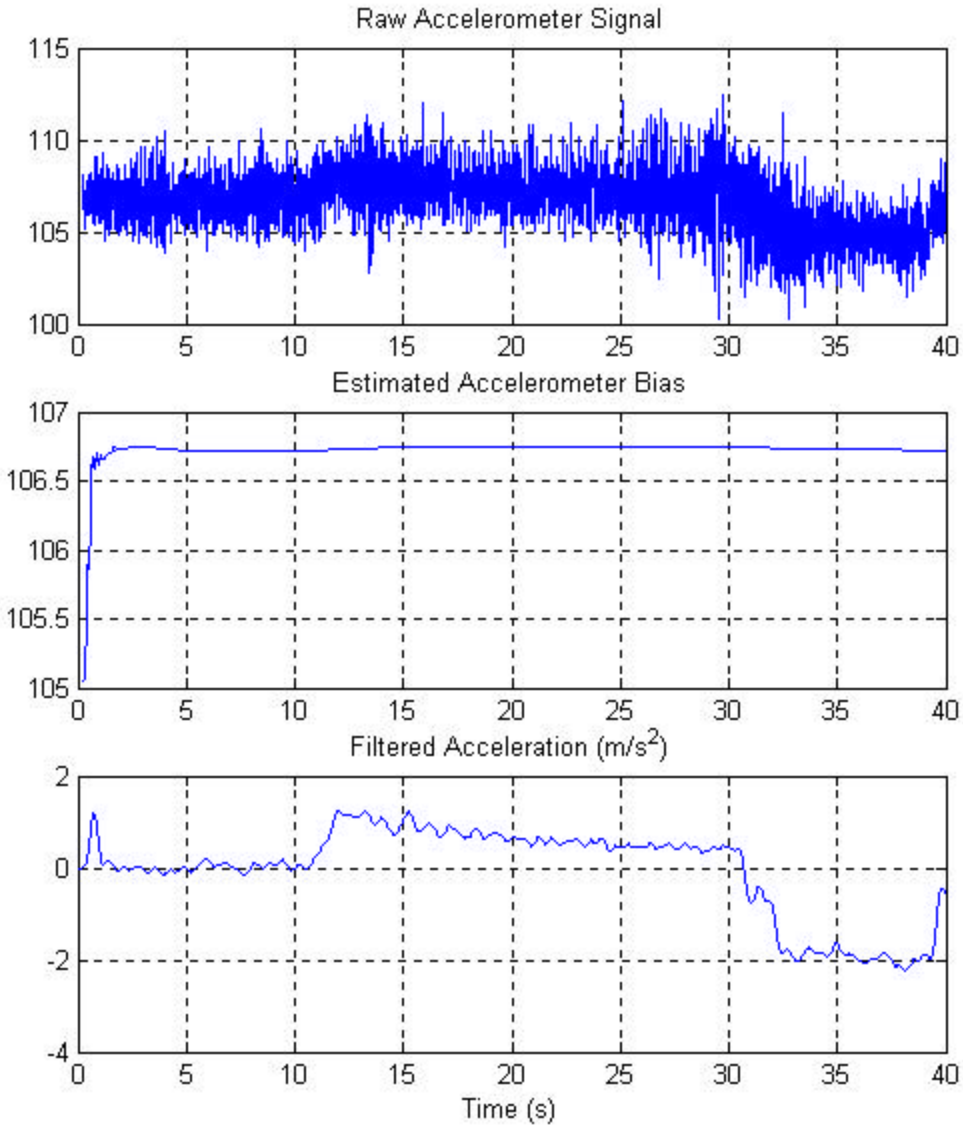

Figure 3.13 Experimental results for accelerometer bias and acceleration estimation

Chapter 4: System Hardware and Software

4.1 Introduction

This chapter describes the system hardware and software that were used to implement the friction coefficient estimation algorithm on the SAFEPLOW. It can be clearly divided into two parts as:

- System hardware: describes the characteristics of all the sensors and devices used in this project.
- System software: describes the software organization and the concrete function of each module.

4.2 System Hardware

In order to experimentally implement the designed friction coefficient estimator in real-time, the SAFEPLOW was equipped with a differential GPS system, an accelerometer, and ABS wheel speed sensors. The Mathworks xPC system was used to serve as the real-time system included a host PC (TOSHIBA 4200 laptop) and a target PC (DELL GX110). The schematic relationship between these devices is shown in Figure 4.1. Each of the components is described in detail in the following sub-sections.

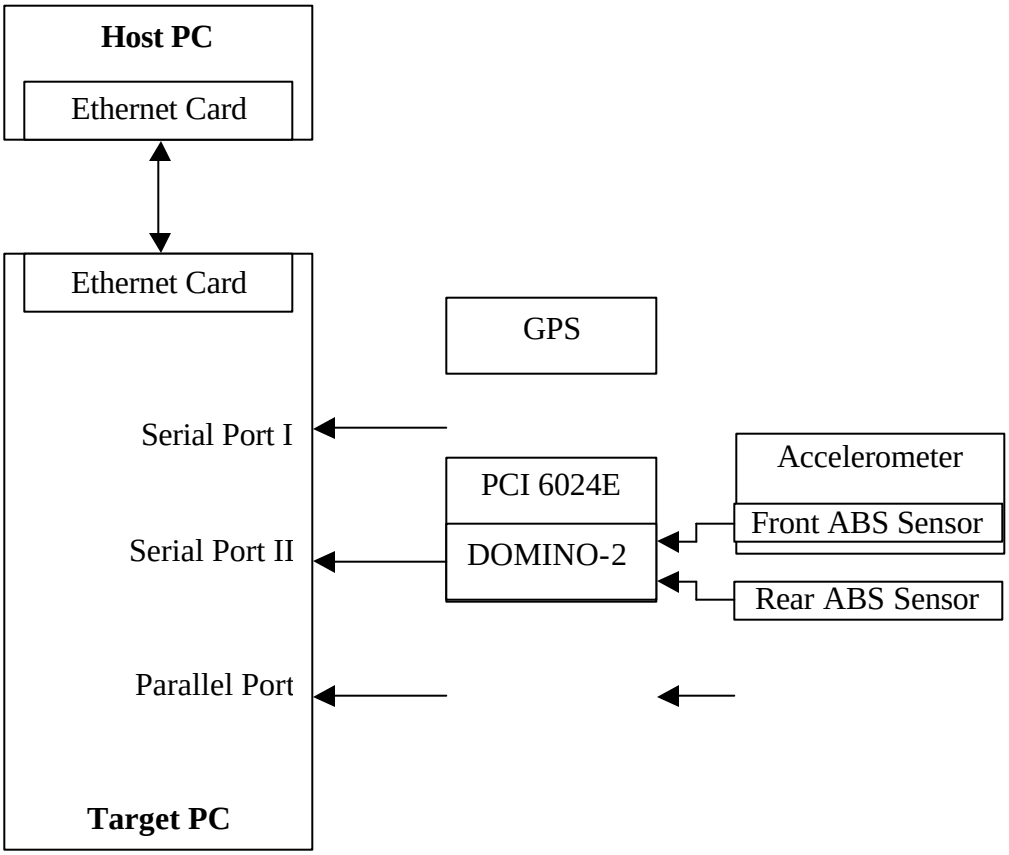

Figure 4.1 Schematic diagram of the system hardware

4.2.1 Accelerometer

The accelerometer used to measure the acceleration/deceleration of the SAFEPLOW in this project is ADXL 105 from Analog Devices. It is a high performance, high accuracy and complete single-axis acceleration measurement system on a single monolithic IC in surface mount package. The ADXL 105 measures acceleration with a full-scale range up to ±5*g* and produces an analog voltage output. The resolution of this accelerometer is 2*mg* and bandwidth is 10KHz. Figure 4.2 shows the accelerometer output signal measured in the still SAFEPLOW. As it indicates, the output signal contains both bias and high frequency noises, which are coped with by the Kalman filter and the digital low-pass filter designed in the previous chapter.

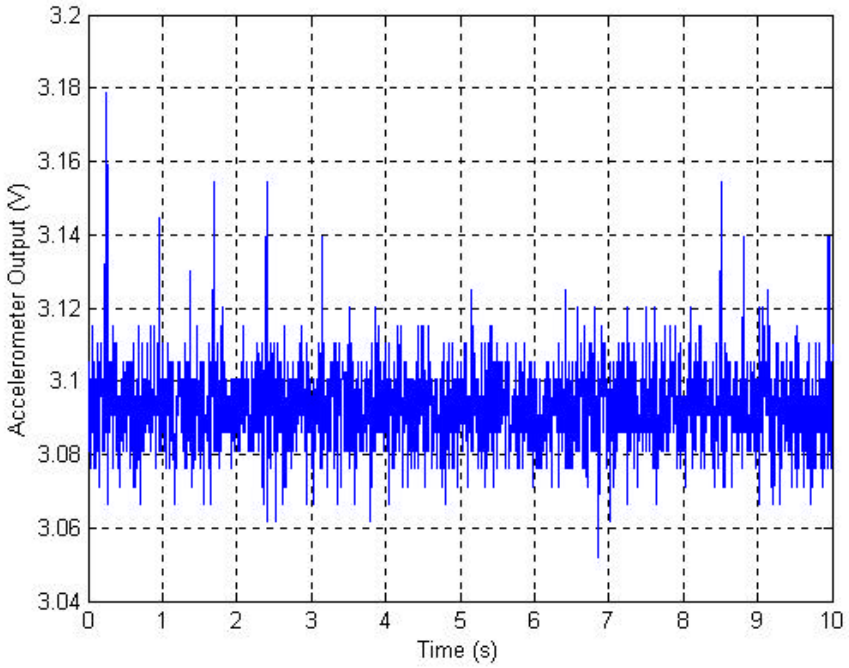

Figure 4.2 Accelerometer output signal in the still SAFEPLOW

4.2.2 DAQ Card

The National Instrument PCI-6024E is served as data acquisition device in this project. The PCI-6024E is an analog and digital I/O system that communicates with a computer through a standard bi-directional parallel port. There are 16 12-bit single-ended analog input channels and 2 12-bit analog output channels; 8 digital I/O channels and two 24-bit counter/timers. The sampling rate for the analog input channel can be as high as 200KHz. The output of the accelerometer is an analog voltage, which is converted into digital signal by PCI-6024E and sent to the computer through parallel port communication.

4.2.3 Differential GPS

The Global Positioning System (GPS) is a satellite-based locating and navigating utility that determines a receiver's precise latitude and longitude by tracking signals from satellites. The GPS constellation of satellites was declared operational in 1995 and

consists of 24 earth orbiting satellites and a set of monitoring and control stations on the ground. The satellites orbit at an altitude of 10,898 nautical miles circling the earth approximately once every 12 hours.

GPS satellites send out two signals: a carrier and a pseudo-random code. The time it takes from the signals to reach the receiver indicates how far away the satellite is. To make position calculations, GPS receivers use signals from four or more GPS satellites. The first three satellites are used to triangulate a position. The fourth is used to improve the positions' accuracy by factoring in the time offset between the satellite system's clock and the GPS receiver's clock.

According to classic GPS theory, one civilian receiver operating in single point mode (no assistance from other sources) will have an accuracy of ±100 meters horizontally. This is far from accurate for this project. Since several errors affecting the signal transmission will be nearly the same for two receivers near each other on the ground, a receiver at a point with known coordinates (the monitor station) can monitor the errors and generate corrections for the remote receiver to use (roving station). This error correction method is called Differential GPS.

Using differential correction along with some additional signal processing involving the phase of the GPS carrier frequencies, the MS750 DGPS system used in this project is typically capable of pinpointing the location of the SAFEPLOW to within ±2.5cm as shown in Figure 4.3.

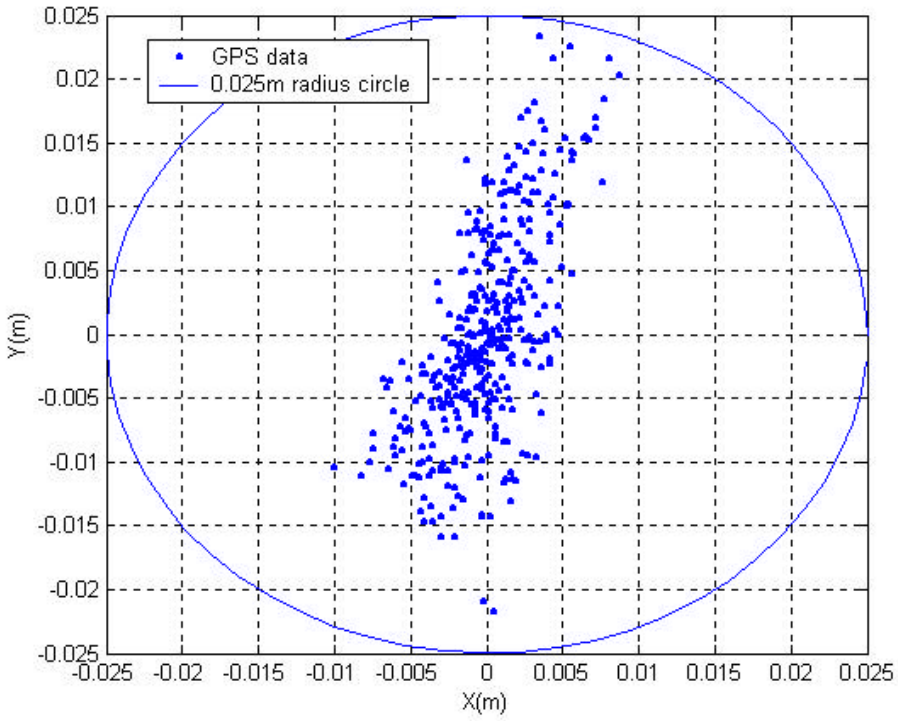

Figure 4.3 DGPS output when the vehicle stands still

The MS750 DGPS system sends out digital data string at 10Hz in serial communication RS232 format. The GGA message string contains the following information:

- Latitude
- Direction of latitude
- Longitude
- Direction of longitude
- GPS Quality indicator
- Number of satellites in use
- Age of differential GPS data record
- Base station ID

The absolute speed of the vehicle can be obtained by differentiating the DGPS position data, which is calculated from the latitude and longitude.

4.2.4 Wheel Speed Sensor and DOMINO-2

In order to calculate the wheel slip (the relative difference between wheel speed and vehicle absolute speed), we need to measure the wheel rotational speed and the vehicle absolute speed. DGPS signal provides a source for the absolute speed. The existing antilock brake system (ABS) sensors on the SAFEPLOW are used to obtain the wheel speeds. There are 100 teeth on each ABS sensor ring. The outputs of the ABS sensors are sinusoidal signals whose magnitudes increase and periods decrease with increasing wheel speed. Therefore, there are 100 periods per wheel revolution. Figure 4.4 shows the output signal of ABS sensor during acceleration.

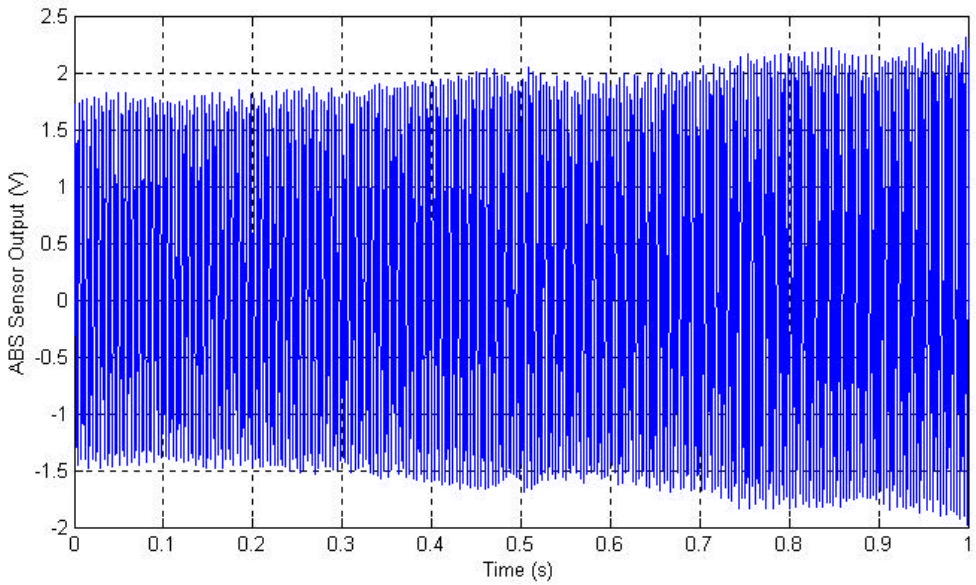

Figure 4.4 The SAFEPLOW wheel ABS output signal

The ABS sensor signals are used to trigger a timer in a micro-controller based system—DOMINO-2 to measure the period of each sinusoidal curve. DOMINO-2 has a 11.059MHz system clock and 2 input interrupt channels. The period measurements of both front wheel and rear wheel are sent to the computer through RS232 serial communication. However, there is a trigger voltage threshold value for the DOMINO-2 system. If the input voltage is too low, it cannot be triggered. Since the ABS output signal voltage magnitude increases with increasing wheel speed, experimental results

show that it is difficult to measure the period accurately if the wheel speed is below 16 rad/s, corresponding to vehicle speed of 15mph.

4.3 System Software

In order to implement the designed friction coefficient estimator on the SAFEPLOW, the whole algorithm including RLS, Change Detection, filters and so on are realized in xPC Target based real-time software.

4.3.1 Real-Time System

The xPC Target version1.3 from Mathworks serves as the real-time operation system for this project. xPC Target is a solution for prototyping, testing, and deploying real-time systems using standard PC hardware. A target PC, separated from the host PC is needed for running real-time applications. The program is first realized in SIMULINK using the standard SIMULINK blocks and then the Real-Time Workshop and a C compiler will create executable code in the host PC. The executable code is downloaded from the host PC to the target PC running the xPC Target real-time kernel through either RS232 serial cable or Ethernet connection. After downloading the executable code, the application can be run and tested in real-time. The main xPC Target features are summarized as follows:

- *Rapid prototyping ability:* the xPC Target can automatically convert the software realized in SIMULINK into executable code, which dramatically cuts the time for coding. In this project, all the software modules are implemented by using standard SIMULINK blocks.
- *High task execution speed:* since the xPC Target is running based on a highly optimized kernel, it makes the target application be capable of high-speed, real-time task execution. A small block model can run with a sample time as fast as 10 μs (100 MHz). Due to model size and system requirement, the sample frequency is chosen as 200 Hz in this project.
- *Convenient signal monitoring and logging:* signal acquisition is through the xPC Target real-time kernel. Signal data for the real-time application is stored in RAM on the

target PC, and can be visualized as curves or numbers and shown in the monitor while a real-time application is running. Moreover, the signal data stored in the target RAM can also be up loaded to the host PC for analysis through RS232 serial communication or Ethernet connection. In this project, the friction coefficient information is displayed on the monitor both numerically and graphically. Ethernet cable is used to connect the target PC and host PC.

4.3.2 Estimation System Software

The friction coefficient estimation system software is composed by several modules. These modules are organized as shown in Figure 4.5. Every individual module is described in detail in the following sub-sections.

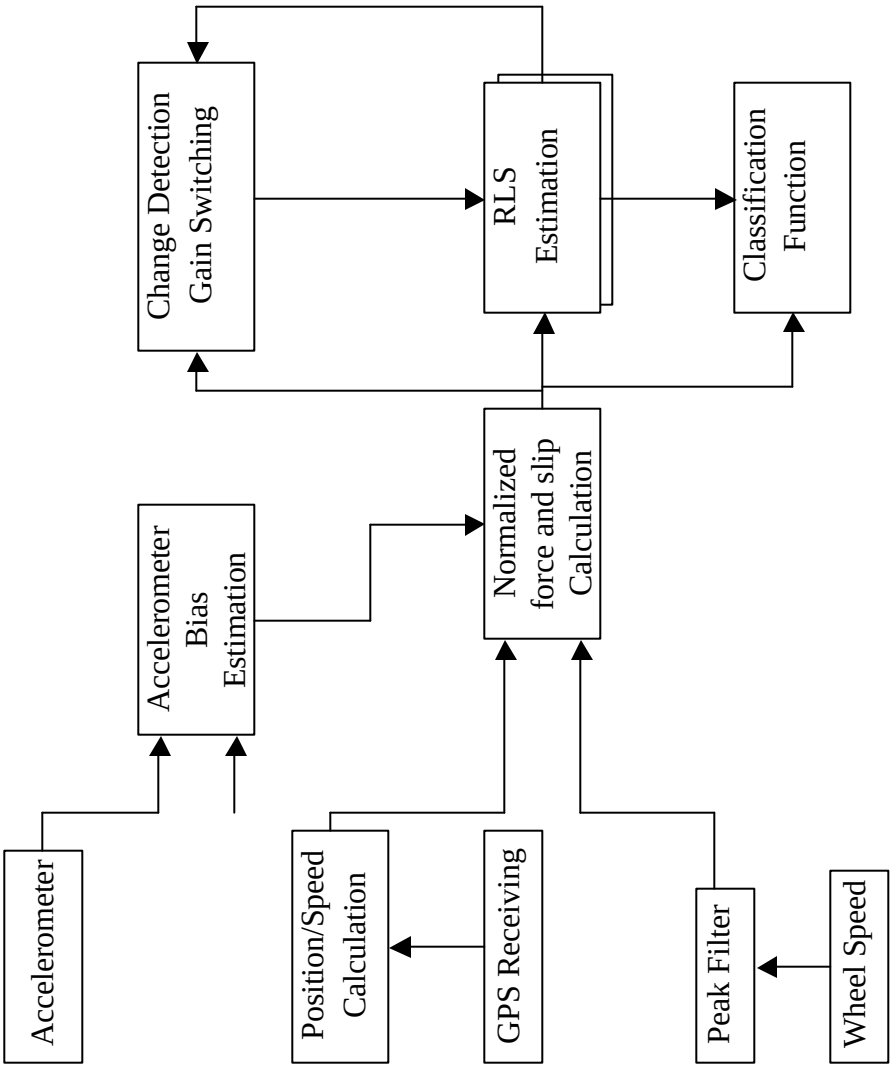

Figure 4.5 Organization of system software modules

4.3.2.1 GPS Receiving Module

Module Inputs: GPS raw data coming from the GPS system.

Module Outputs: longitude, latitude of the vehicle and GPS time.

The GPS module is used to receive the GPS signal from RS232 serial port COM1. The main functions of the GPS module are:

1. Initialize serial port COM1 for GPS communication and specify the data types according to the structure of GPS signal frame.
2. Receive raw GPS data string from GPS system.
3. Parse the raw GPS data string and extract the longitude, latitude, and GPS time information.
4. Send the extracted data to the position/speed calculation module.

The xPC RS232 Mainboard receiver module is used to receive the GPS signal. The serial communication Baudrate is set as 9600 Hz. The GPS signal format is GGA with updating rate as 10 Hz. 16 output pins are specified for the RS232 Mainboard receiver according to the data structure of the GPS raw data string. The longitude, latitude, and GPS time are extracted and sent to the position/speed calculation module at once a complete GPS frame is well received.

4.3.2.2 Position/Speed Calculation Module

Module Inputs: GPS time, latitude, and longitude.

Module Outputs: vehicle current position in X and Y coordinate, and vehicle speed.

The main purposes of the module are:

1. Interpret the longitude and latitude information as X and Y coordinate.
2. Numerically differentiate the X and Y, and calculate the speed.

The longitude and latitude information parsed in the GPS module are first converted into global X and Y coordinate. And then, the X and Y are numerically differentiated in the following way:

$$\dot{X} = \frac{X_c - X_p}{T_{GPSc} - T_{GPSp}} \tag{4.1}$$

$$\dot{Y} = \frac{Y_c - Y_p}{T_{GPSc} - T_{GPSp}} \tag{4.2}$$

where, X_c, Y_c are the current vehicle coordinates, X_p, Y_p are the vehicle coordinates in the previous cycle. T_{GPSc} and T_{GPSp} are the current GPS time and previous GPS time, respectively. After obtaining the $\dot{X}$ and $\dot{Y}$, the vehicle speed can be calculated as:

$$V = \sqrt{\dot{X}^2 + \dot{Y}^2} \tag{4.3}$$

Since the GPS signal is updated at frequency about 10 Hz, the output of the module, X, Y, and V are updated about every 0.1 second.

4.3.2.3 Wheel Speed Module

Module Inputs: output signals from DOMINO-2 microprocessor.

Module Outputs: vehicle front and rear wheel speeds.

The main functions of the module are:

1. Parse the signals from DOMINO-2 into front and rear wheel pulse period signals, respectively.
2. Calculate the front and rear wheel speeds based on the measured pulse periods.

The front wheel ABS signal and rear wheel ABS signal are connected to the two input channels of the DOMINO-2, respectively. There are two outputs from the DOMINO-2. The first output is the channel identifier, with the value of "1" or "2", which indicates the measured pulse period in the second output belong to either channel1 or channel2. The second output of the DOMINO-2 is the measured pulse period value with resolution as 1.085 ms. Since there are 100 teeth on both the front and rear wheel tracks, 100 pulses will be generated per wheel revolution. Thus, the wheel speed can be calculated as follows:

$$w_{f,r} = \frac{2p}{100 \times 1.085 \times 10^{-6} \times P_{m\_f,r}} \tag{4.4}$$

where, $w_{f,r}$ represents the front and rear wheel speeds. $P_{m\_f,r}$ represents the measured pulse periods for front and rear wheel.

4.3.2.4 Wheel Speed Peak Filtering Module

Module Inputs: measured front and rear wheel speeds, GPS speed.

Module Outputs: filtered peak-free front and rear wheel speeds.

The main function of this module is to eliminate the big peaks contained in both the front and rear wheel speed signals. The peak filter driven by the GPS speed signal designed in the previous chapter is implemented in this module. This module will function only if the GPS speed is in the regular interval of [3 m/s, 30 m/s].

4.3.2.5 Accelerometer Bias Estimation Module

Module Inputs: raw accelerometer signal, GPS speed.

Module Output: acceleration/deceleration.

The main functions of the module are:

1. Estimate the accelerometer bias on-line.
2. Remove the bias and high frequency noise in the accelerometer signal.

The Kalman filter designed in the previous chapter is implemented in this module to estimate the accelerometer bias. The estimated bias is removed from the accelerometer signal and then a digital elliptic low-pass filter attenuates the high frequency noises. This module is also controlled by the GPS speed. It will function only if the GPS speed is in the regular interval of [3 m/s, 30 m/s].

4.3.2.6 Normalized Force and Slip Calculation Module

Module Inputs: GPS speed, vehicle acceleration/deceleration, front and rear wheel speeds.

Module Outputs: regression vector, and measured system output.

As the preparation part for the RLS module, the main functions of this module are:

1. Calculate the slip for both front wheel and rear wheel using the front and rear wheel speed and GPS speed (vehicle absolutely speed).
2. Calculate the normal force for both front and rear wheels.

3. Calculate the traction/braking forces generated at both front and rear wheels based on the vehicle dynamics.
4. Switch the appropriate calculate results as the regression vector and measured system output—module outputs.

The slips, regression vector, and the measured system output (Normalized force) are calculated according to the models described in chapter 2. The vehicle acceleration/deceleration signal is used as the switching signal, which controls whether the traction calculation results or the braking calculation results go to the module outputs based on its polarity (positive for traction and negative for braking).

4.2.2.7 Change Detection/Gain Switch Module

Module Inputs: vehicle acceleration, wheel speed, measured system output, estimated system output, and drift.
Module Output: RLS gain
The main functions of this module are:
1. Monitor the identification error and generate alarm signal if the road surface is changing.
2. Switch the proper gain for the RLS module to ensure it has less variation when there is no road surface changing and prompt convergence rate when there is road surface changing.

The CUSUM change detection algorithm described in chapter 3 is implemented in this module. The alarm signal triggers the gain switching mechanism. If a change is detected, a big gain will be switched to the module output, and resume to regular gain when the alarm signal disappears. The force calculation will become inaccurate if the vehicle acceleration/deceleration is too small, and the ABS signal will become very inaccurate below certain speed, therefore, the vehicle acceleration/deceleration and wheel speed signals are used to determine whether the RLS should update the friction information or not. If one of these two signals is below certain level, the RLS gain will

be switched as zero, and the system stops update the friction information and keeps the old value.

4.2.2.8 RLS Module

Module Inputs: regression vector, measured system output, gain.

Module Output: estimated slip-slope.

The main function of this module is to update the estimated slip-slope value in real-time based on the inputs and the gain provided by the Change Detection/Gain Switch module. The RLS algorithm described in chapter 3 is implemented in this module.

4.2.2.9 Road Surface Classification Module

Module Inputs: estimated slip-slope, normalized longitudinal force, wheel slips.

Module Output: road surface friction level.

The main function of this module is to classify the road surface friction level based on the estimated slip-slope or normalized longitudinal force and measured wheel slips using a classification function, which is developed based on the experimental data. If the slip is low, the slip-slope is used to classify the road surface friction level. If the slip is high, the normalized longitudinal force is directly used to classify the friction level.

Chapter 5: Experimental Results

5.1 Introduction

After designing the estimation algorithm, extensive experimental tests were carried out to improve and verify the estimation system performance. This chapter presents and analyzes the experimental results.

As described in chapter 2 and chapter 3, the objective of the friction coefficient identification system is to estimate the road surface friction level or the maximum friction coefficient m_m that the tire-road can provide during both vehicle acceleration (traction) and braking maneuvers. Many tests were done on different road surfaces for different operations. This chapter consists of the following parts:

- Experimental results on dry concrete road surface, including both acceleration and braking.
- Experimental results on concrete surface with light snow covering, including both acceleration and braking.
- Experimental results on road surface that consists of two different friction levels, which are used to examine the system transient response.
- Experimental result for hard braking in which the tires undergo high slip and work in the nonlinear region of the friction-slip relationship.
- Analysis of the experimental results.

The vehicle used to conduct the experiments is a full sized snowplow (referred to as SAFEPLOW) manufactured by Navistar International Truck Company as shown in Figure 5.1. This SAFEPLOW is equipped with GPS antenna/receiver, ABS, accelerometer, radar, and several other sensors and actuators.

Figure 5.1 The SAFEPLOW used for the experiments

The main parameters of this SAFEPLOW related to the longitudinal dynamics for the friction coefficient identification are listed in Table 5.1.

Parameter	Total Mass (Kg)	L_f (m)	L_r (m)	Height of C.G. (m)	Vehicle Front Area (m^2)
Value	9834	2.339	2.716	1.2	6.0

Table 5.1 SAFEPLOW main parameters

5.2 Tests on Dry Concrete Road Surface

The experiments for this part were carried out on the dry concrete testing track at the MnRoad Research Facility on sunny days. The track was well-paved concrete surface and completely dry. So, the friction level of the surface was very good. The maximum friction coefficient m_m is around 1.

5.2.1 Acceleration (Traction) Test

The slip-slope based friction coefficient estimation method was conducted for acceleration with different starting speeds. At the beginning of the test, the speed of the vehicle was kept constant for about 6 seconds to allow the low-pass filters to initialize and Kalman filter to estimate the accelerometer bias. After that, the vehicle starts accelerating. Figure 5.2 and Figure 5.3 show the slip-slope estimation results for acceleration with starting speeds at 20 mph (9 m/s) and 25 mph (11 m/s), respectively. As the results indicate, the slip-slopes for the dry concrete acceleration converge to a value of about 9.8.

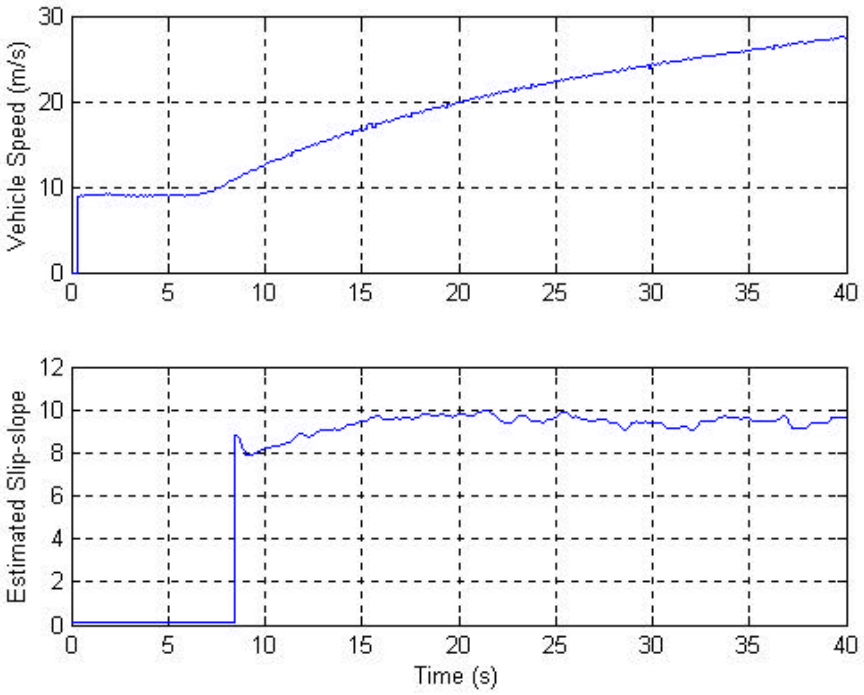

Figure 5.2 Acceleration starting at 20mph on dry concrete surface

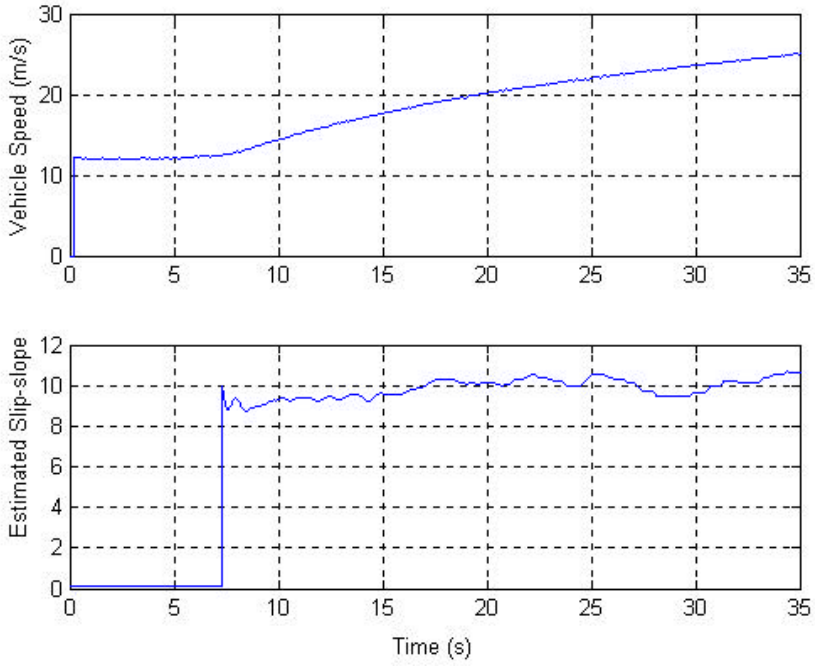

Figure 5.3 Acceleration starting at 25mph on dry concrete surface

5.2.2 Combination of Acceleration and Braking Test

Experiments for the situation of sequential acceleration and braking were also studied on the same dry concrete surface. Figure 5.4 shows one of the testing results. The SAFEPLOW first stays at a constant speed for a while to let the filters initialize and estimate the accelerometer bias, then it starts accelerating for about 20 seconds and then gently brakes for about 10 seconds. As the result indicates, the slip-slope consistently converges to about the same value around 9.8.

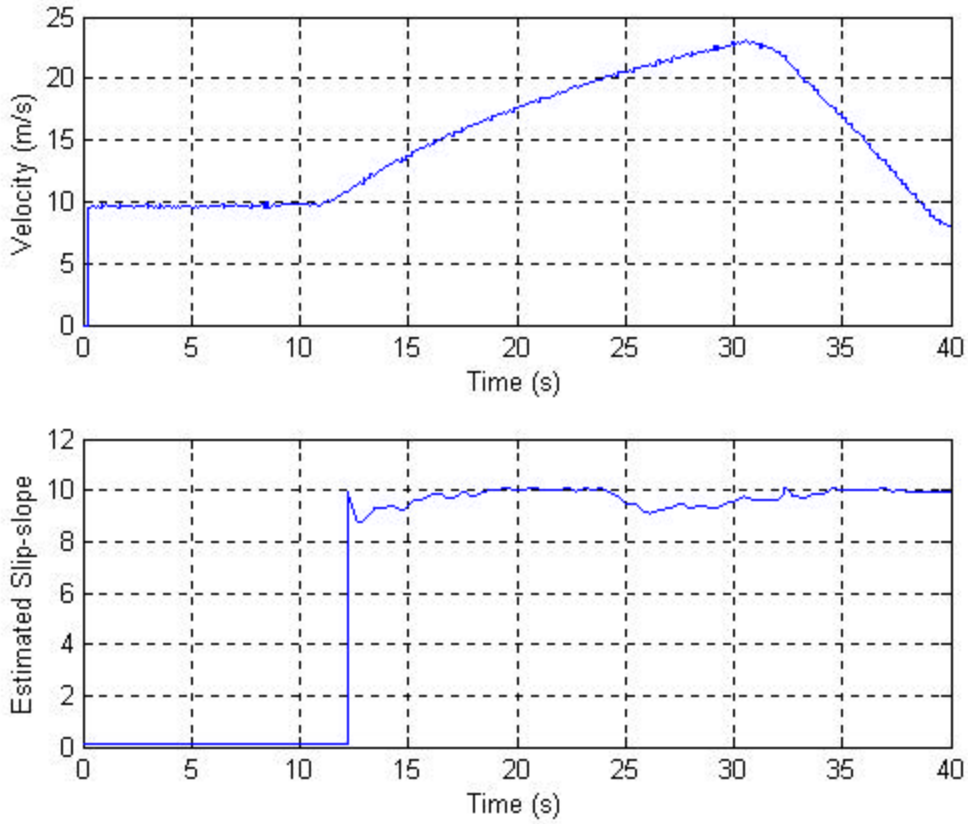

Figure 5.4 Slip-slope estimation during acceleration and braking

From the experimental results, we can see that for acceleration and braking in the small slip region, the slip-slope consistently converges to some value around 9.8 on this surface. Therefore, we can use this slip-slope value to classify the road surface as dry concrete, dry concrete like surface or classify the maximum friction coefficient m_m as about 1.

5.3 Tests on Concrete Surface with Light Loose Snow Covering

The experiments for this part were carried out also on the concrete testing track at the MnRoad Research Facility, but on a day after a heavy snow day. The track had already been plowed, but since no salt and sand were put on it, it was still lightly covered by loose snow brought on by wind. Figure 5.5 shows the exact road surface condition for the experiments presented in this section. The right side lane in the figure was used for the testing. Since the road surface is slightly slippery, the maximum friction coefficient m_m is expected to be less than 1.

Figure 5.5 The road surface used to conduct the experiments for this section

5.3.1 Acceleration (Traction) Test

Similar to the tests in section 5.2.1, the slip-slope based friction coefficient estimation method was used for acceleration with different starting speeds on this surface with light snow covering. Figure 5.6 and Figure 5.7 show the slip-slope estimation results for acceleration with starting speed as 20 mph (9 m/s) and 25 mph (11 m/s), respectively. As the results indicate, the slip-slopes for the acceleration converge to a value about 7.0.

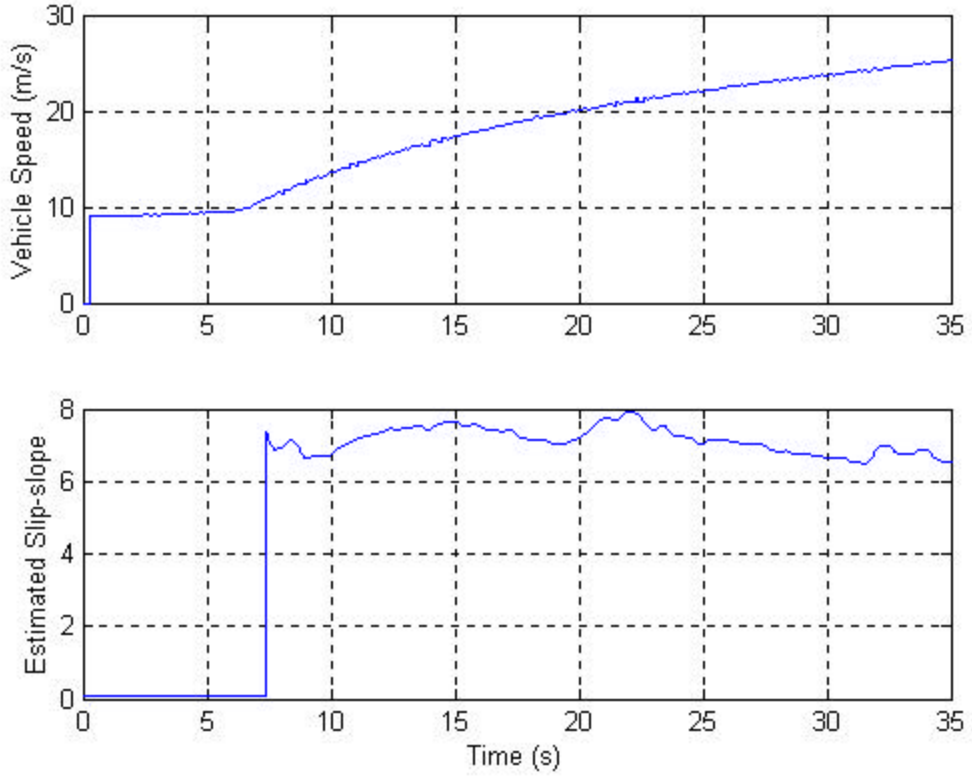

Figure 5.6 Acceleration starting at 20mph on surface with light covering snow

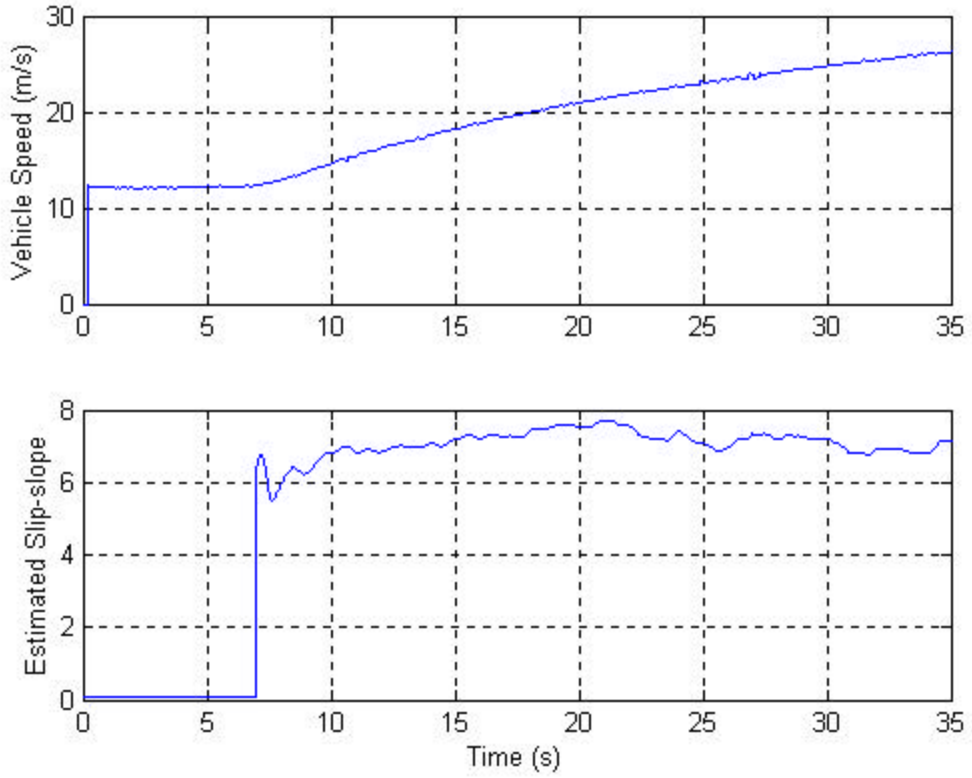

Figure 5.7 Acceleration starting at 25mph on surface with light covering snow

5.3.2 Combination of Acceleration and Braking Test

Similar to the tests in section 5.2.2, experiments for the situation of sequential acceleration and braking were also conducted on the same concrete surface. Figure 5.8 shows one of the testing results. The SAFEPLOW first stays at a constant speed for a while to let the filters initialize and estimate the accelerometer bias, then it starts accelerating for about 16 seconds and then gently brakes for about 16 seconds. As the result indicates, the slip-slope consistently converges to about the same value around 7.0.

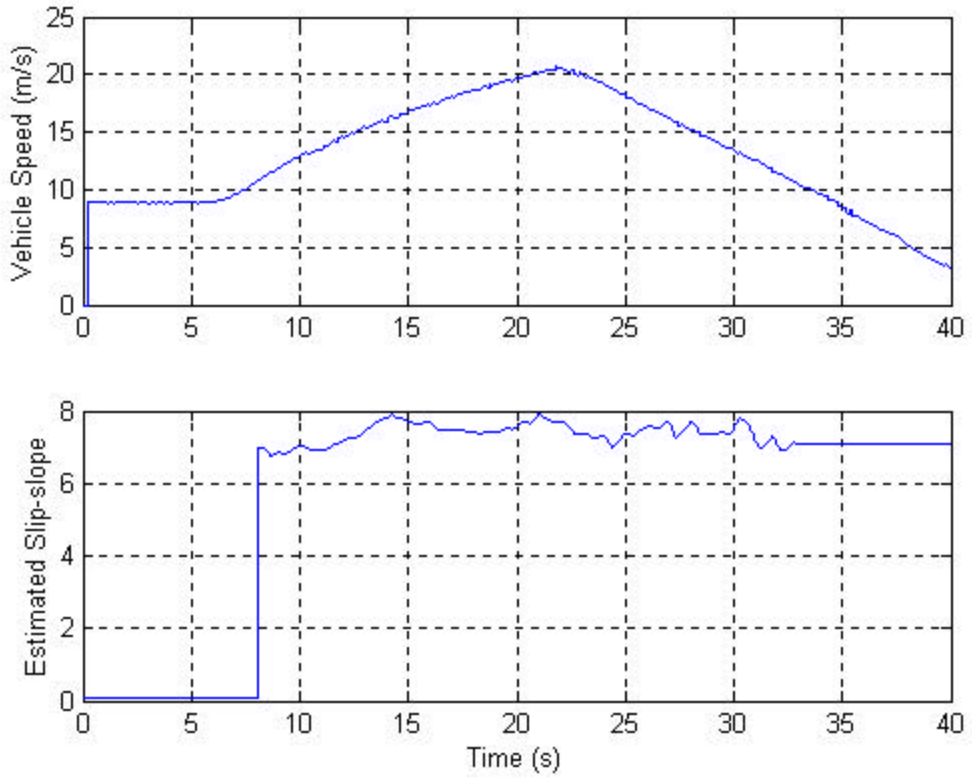

Figure 5.8 Acceleration and braking on surface with light covering snow

Notice that the estimator stops updating the slip-slope at about 32 seconds because the wheel speeds are below the threshold value that Domino-2 can detect. Thus, the system just keeps the last estimated value before stopping the updating.

From the experimental results, we can see that for acceleration and braking in the small slip region, the slip-slope consistently converges to some value around 7.0, which is quite different from the slip-slope value (9.8) obtained on dry concrete surface. Therefore, we can use this slip-slope value to classify the road surface as a slightly slippery surface or the maximum friction coefficient m_m as about 0.7.

5.4 Tests on Surface Consisting of Two Different Friction Levels

The purpose of the experiments in this section is to test the system transient response performance and ability to detect the sudden change of the road friction level. The tests were conducted on a track at Minnesota Highway Safety and Research Center (St. Cloud, Minnesota). The testing track consists of two surfaces with different friction levels — dry asphalt surface and icy surface. Figure 5.9 shows the transitional part of the track.

Figure 5.9 The track used to conduct the experiments for this section

5.4.1 Acceleration (Traction) Test

The SAFEPLOW was started at 15 mph and accelerated through the transitional part of the testing track. The result is shown in Figure 5.10. At the beginning, the SAFEPLOW keeps constant speed and therefore, the system does not update the friction coefficient. At about 14 seconds, it starts accelerating on the dry asphalt and the system starts updating the friction coefficient. The third row of the Figure 5.10 shows the slip value of the tire. On the dry asphalt surface, the slip is low and the tires work in the linear region, therefore, the slip-slope is used to classify the surface friction level. At once the vehicle

hits the icy surface, the tire slip increases significantly and the tires work in the nonlinear region, therefore, the normalized force is used to classify the surface friction level.

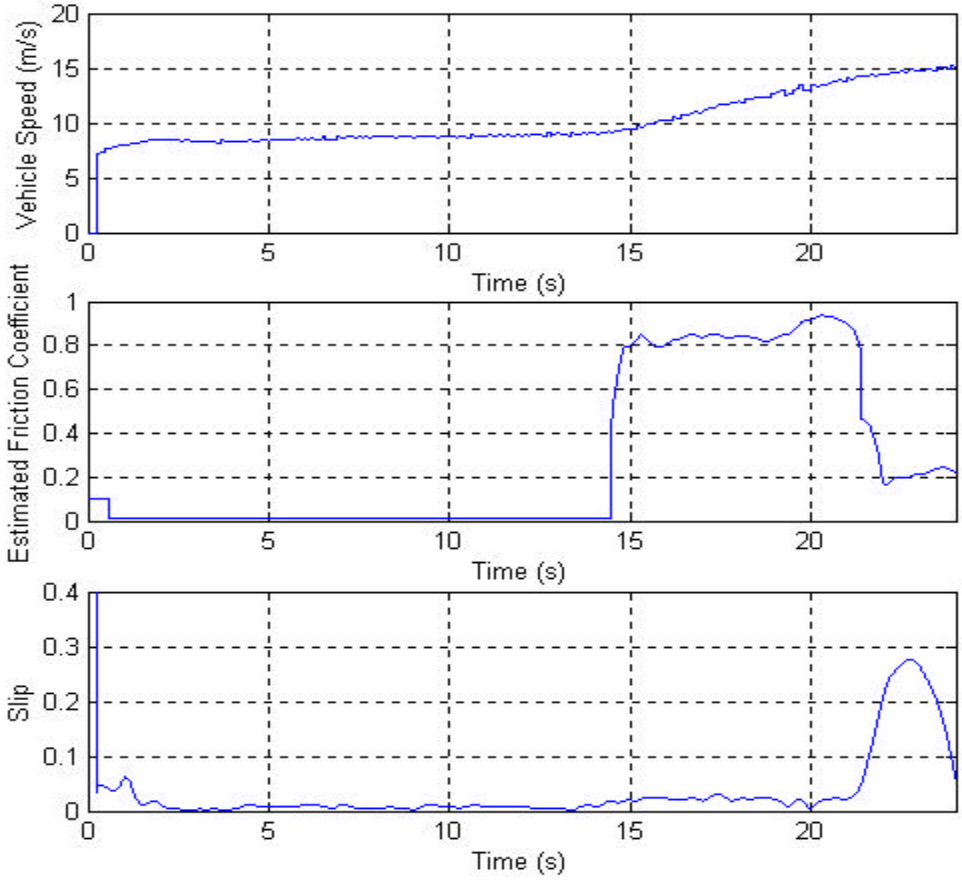

Figure 5.10 System response when accelerating through the transitional part

As the result indicates, the system can promptly detect the sharp change on the road surface friction level and the friction coefficient converges to 0.22 for the icy surface.

5.4.2 Combination of Acceleration and Braking Test

Figure 5.11 shows the experimental result of the testing in which the SAFEPLOW accelerates on the dry asphalt surface and brakes through the transitional part of the track. Similarly, on the dry asphalt surface, tires work in the low-slip linear region and the slip-slope is used to classify the surface friction level for both acceleration and braking.

However, the wheel will lock up at once it reaches the icy surface when performing brake. Thus, the slip will be almost as high as 100% and the tires are working in the nonlinear region, therefore, the normalized force is used to classify the surface friction level. As the result indicates, the system promptly converges the friction coefficient to 0.22 at once the vehicle reaches the icy surface.

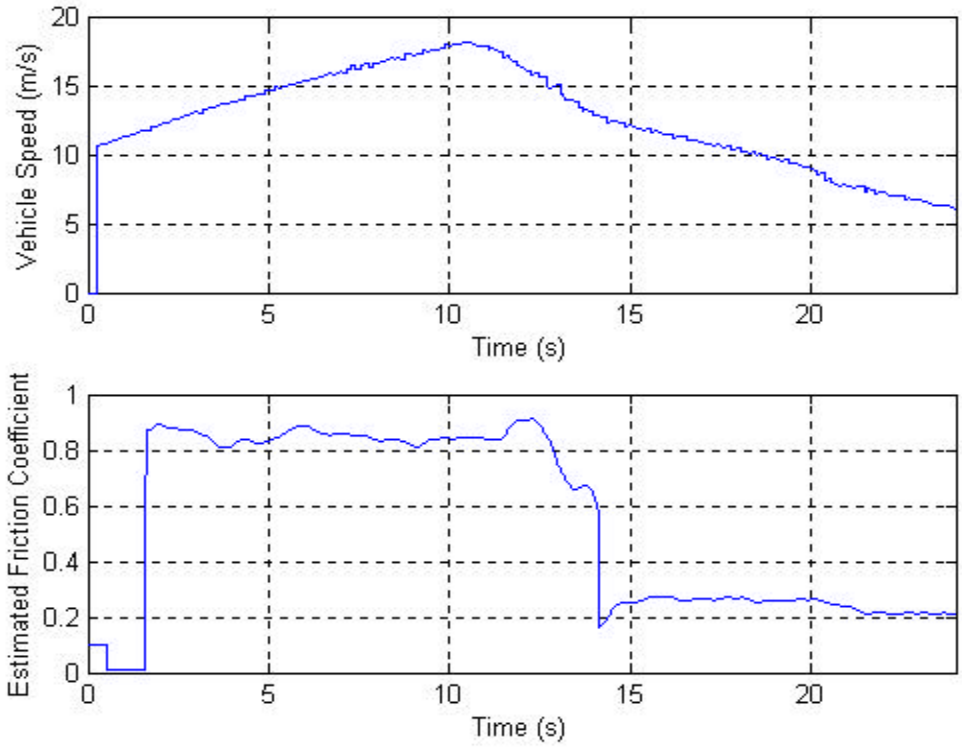

Figure 5.11 System response when braking through the transitional part

5.5 Hard Braking Test

This section is used to further verify the system performance in high-slip region (nonlinear part of the friction-slip curves). SAFEPLOW performs hard braking on dry concrete surface at MnROAD Research Facility. Figure 5.12 shows the testing result. Since the tires are working outside the linear region, the normalized force is directly used to classify the surface friction level. As the result indicates, the system behaviors well

even in the nonlinear region. The estimated friction coefficient converges to about 0.96 at once the vehicle starts hard braking.

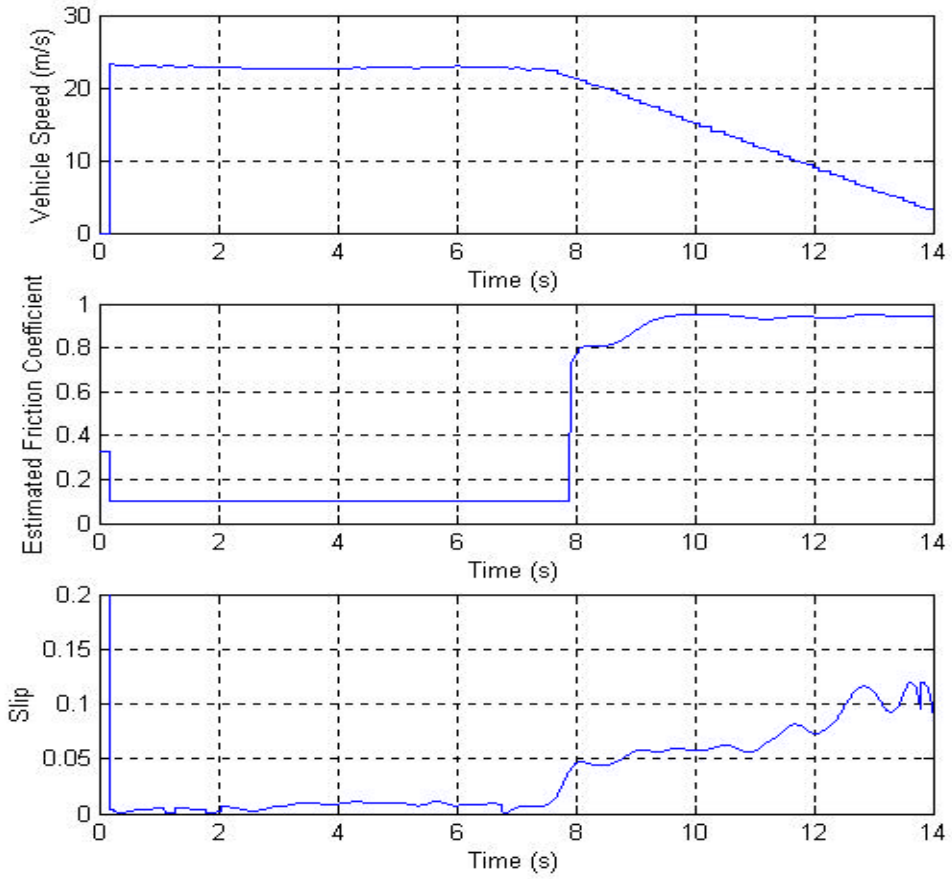

Figure 5.12 Testing result for hard braking

5.5 Tests on a Gravel Surface

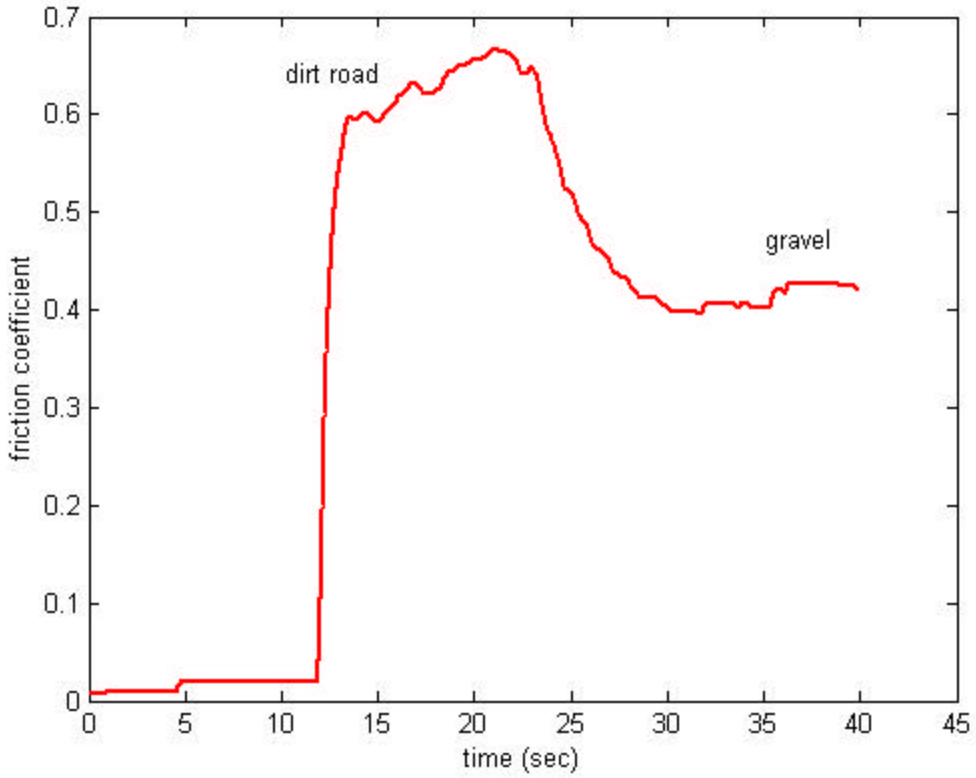

Figure 5.13 Estimated friction coefficient on a gravel road surface

Figure 5.13 shows the estimated friction coefficient on a dirt road and on a gravel surface. Once the snowplow starts accelerating around 12 seconds, the friction coefficient is initially estimated to be around 0.6 while the vehicle is on a dirt road. Later when the vehicle moves to a gravel surface, the friction coefficient is estimated to be around 0.4

5.6 Analysis of the Experimental Results

The friction coefficient estimation system was analyzed in detail to determine the reasons that limit the system performance and methods to improve it. The following reasons were found that limited the system performance:

1. Sensitivity of the accelerometer to the vertical vibration. In the experiments, an accelerometer is attached on the vehicle body along its longitudinal axis to measure the total longitudinal acceleration/deceleration of the vehicle. However, in the testing, we found that the accelerometer not only responds the longitudinal acceleration/deceleration as expected, but also slightly reacts to the vertical vibrations caused by road surface roughness and engine. The accelerometer output signal caused by the vertical vibrations is in the same frequency band as the longitudinal acceleration/deceleration. Thus, it is hard to remove this noise from the signal using filters. This contaminated acceleration/deceleration definitely will cause fluctuation of the estimated slip-slope. Figure 5.14 shows the measured and filtered accelerometer signal when the SAFEPLOW is running at a constant speed, 9 m/s on a well-paved flat concrete surface. As one can see, the accelerometer still has considerable response even the vehicle is running at a constant speed on a quite flat road surface. If the road surface is bumpy, the accelerometer will pick up more significant noise due to vehicle vertical vibrations.

This issue might be ameliorated if we calculate the traction force from engine, transmission, driveline, and brake system dynamics. However, this method would require more sensors and measurements, which are not accessible in this project.

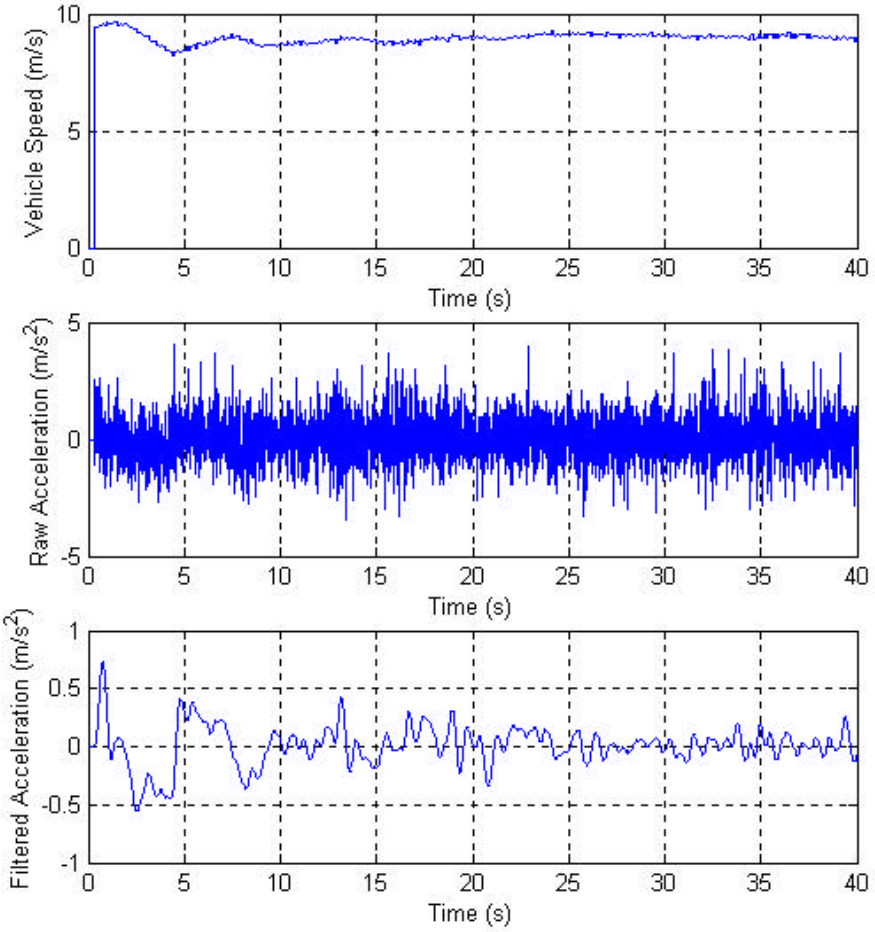

Figure 5.14 Measured and filtered accelerometer signal at constant vehicle speed

2. Wind speed influence. In the longitudinal force calculation of chapter 2, the air drag force is set as $F_a = D_a V^2$ with ignoring the wind speed. However, in case of windy weather conditions, the air drag force would be $F_a = D_a (V + V_w)^2$, with V_w being the wind speed. However, we could not measure the wind speed on the SAFEPLOW and the wind speed is set as 0 in the experiments, which could introduce some error in the longitudinal force calculation especially during windy days. In the experimental testing, we tried to avoid the windy days, however, in the practical applications, the ignoring of the wind speed could still cause some error. In order to obtain a more accurate F_a, a wind speed sensor is needed to measure the V_w.

3. DOMINO-2 trigger threshold voltage value. In this project, the wheel speed is calculated from the ABS wheel speed sensor signal of the SAFEPLOW. As shown in chapter 4, the ABS wheel speed sensor output is a sinusoidal signal whose period is proportional to the speed and magnitude increases with speed as well. The DOMINO-2 microprocessor is used to capture the rising edges of the signal and therefore to calculate the signal period and wheel speed. However, in order to trigger the DOMINO-2, the voltage of the signal needs to be bigger than a threshold value (about 2v), and thus the signal period can be precisely calculated. We experimentally found that the wheel speed has to be above 16 rad/s to ensure adequately accurate slip calculation. If the wheel speed is too low, the slip will be inaccurate and neither the slip-slope. However, this limitation could be overcome by using a more sensitive microprocessor or better ABS sensor.

4. Slow GPS sampling rate. The GPS system we used in the project provides samples at 10 Hz. The vehicle speed is obtained from the differentiation of this GPS signal. The sampling rate of the whole system is 200 Hz. That means the speed signal updates only 1 time while other signals update 20 times. If the vehicle travels at 20 m/s, then the estimator will get a new speed signal every 2 meters. This low GPS sampling rate certainly introduces lag into the system. A faster GPS could improve the system performance.

Chapter 6: Instrumented Redundant Wheel for Friction Measurement

6.1 Friction Wheel

A new friction measurement system consisting of a redundant wheel mounted at a small angle to the longitudinal axis of the vehicle was developed. This wheel-based system was found to be a good candidate for a robust, reliable and inexpensive friction measurement system. The system requires no actuators and requires no skidding. Since it is mounted at an angle to the vehicle axis, the wheel always has an adequate slip angle and was able to reliably estimate friction coefficient.

This redundant wheel-based system must be contrasted with the Norse meter, a friction meter manufactured by Norsemeter Company, Rud, Norway. The Norse meter also utilizes a redundnat wheel (an automobile tire) attached to the truck. This tire is automatically skidded on the roadway surface at timed intervals (and at the operator's discretion) and a friction value is recorded by the Norsemeter. The disadvantages of the Norse meter are

1) Problems with corrosion of parts, broken belts and frequent replacement of failed components.
2) The Norsemeter is expensive. Each device costs over $50k.

Unlike the Norse meter, the friction wheel developed in this project has very few moving parts, no actuators for skidding and requires no braking of the wheel. It is expected to be much more reliable than the Norse meter and also much less expensive. The approximate cost of all the components used in the development of the prototype wheel for this project was less than $2000.

Figure 6.1 shows a photograph of the instrumented wheel on the Safeplow. The wheel is pivoted and attached to the snowplow through a load cell. Lateral forces on the wheel are transmitted to the snowplow through the load cell. A pneumatic actuator is used to apply a constant vertical load on the tire. The pneumatic actuator utilizes the spare tank of compressed air on the snowplow.

Figure 6.1 Instrumented redundant wheel

Figure 6.2 Friction wheel when it is lifted off the road

Figure 6.3 Regulator that controls vertical pneumatic force on friction wheel

Figure 6.2 shows a photograph of the friction wheel when it has been withdrawn and lifted off the road. A switch near the driver's seat activates the pneumatic actuator and is used to deploy the friction wheel or to lift it off the road. Figure 6.3 shows the regulator system that is used to control the vertical pneumatic force on the wheel.

6.2 Experimental Results

The friction wheel was evaluated on dry asphalt road, on gravel and during transitions from gravel to asphalt road and vice-versa. Figure 6.4 shows experimental data on dry asphalt road at low speed. The friction coefficient was calculated directly from the lateral force measured by the load cell on the friction wheel. As seen in Figure 6.4, once the snowplow starts moving, the friction coefficient is measured to be a value around 0.85. There is significant noise in the readings, which come from the vibrations of the snowplow. The effect of the noise could potentially be removed in the future by signal processing algorithms that utilize additional vibration sensors.

Figure 6.5 shows the friction coefficient measured by the friction wheel on dry asphalt at a vehicle speed of 25 mph. Again it can be clearly seen that the mean value of the measured friction coefficient is around 0.85, though there is significant variation from the mean due to noise in the measurement.

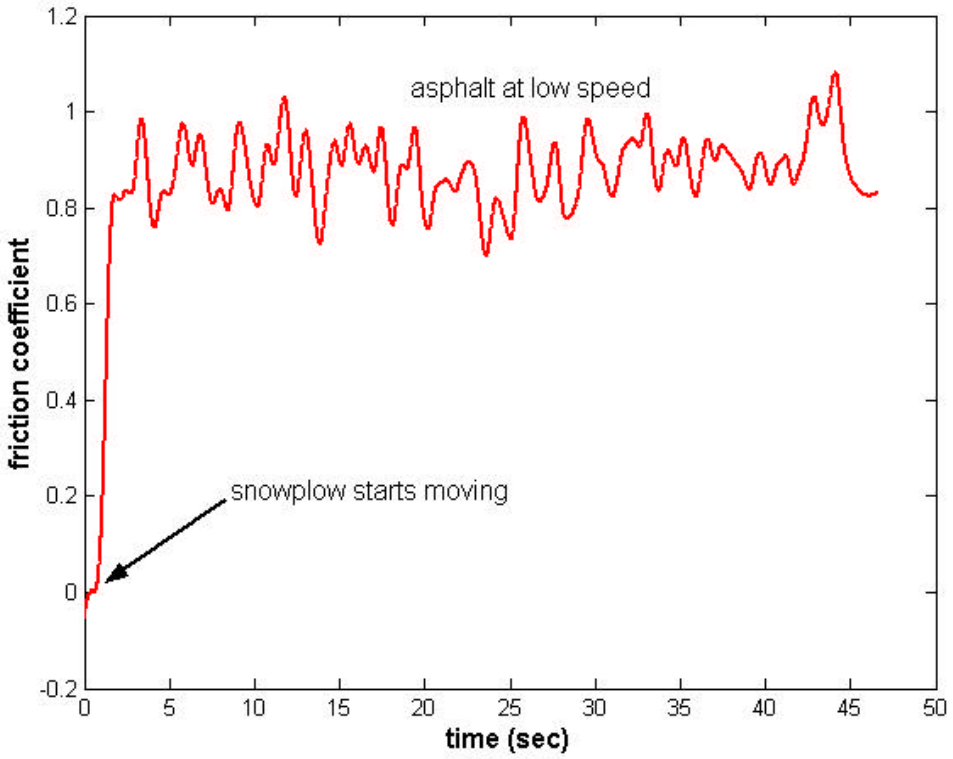

Figure 6.4 Friction coefficient on dry asphalt road at low speeds

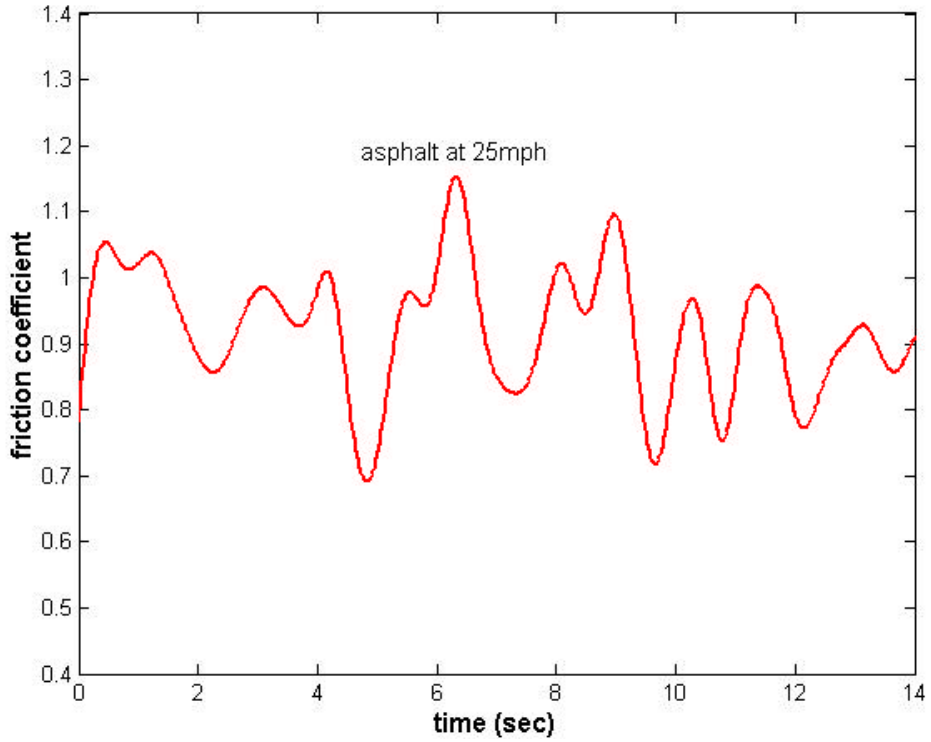

Figure 6.5 Friction coefficient on dry asphalt road at 25mph

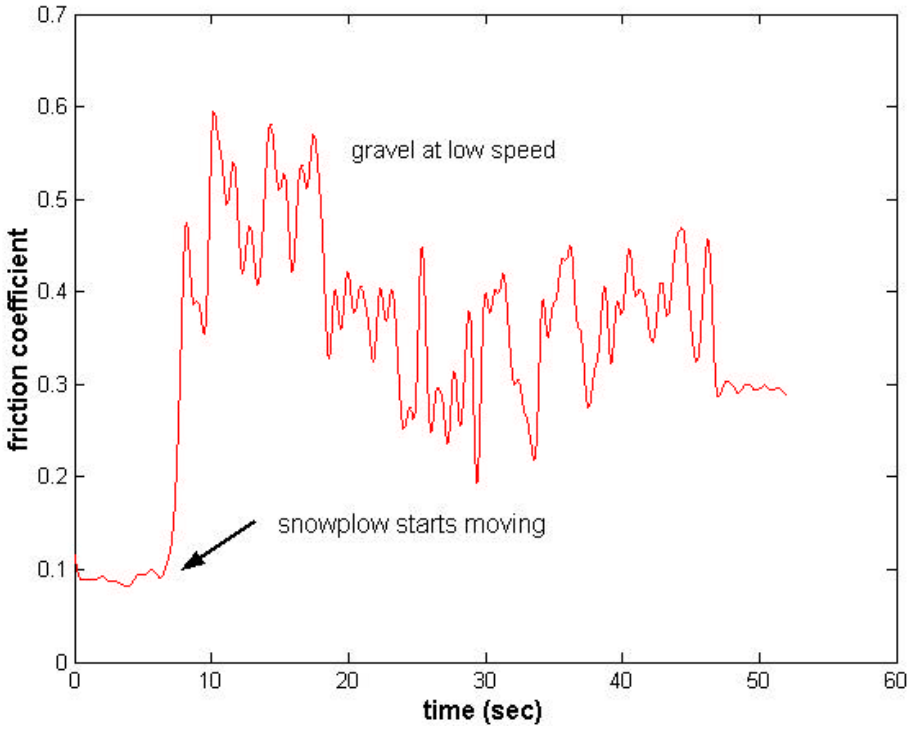

Figure 6.6 Friction coefficient on gravel road at low speeds

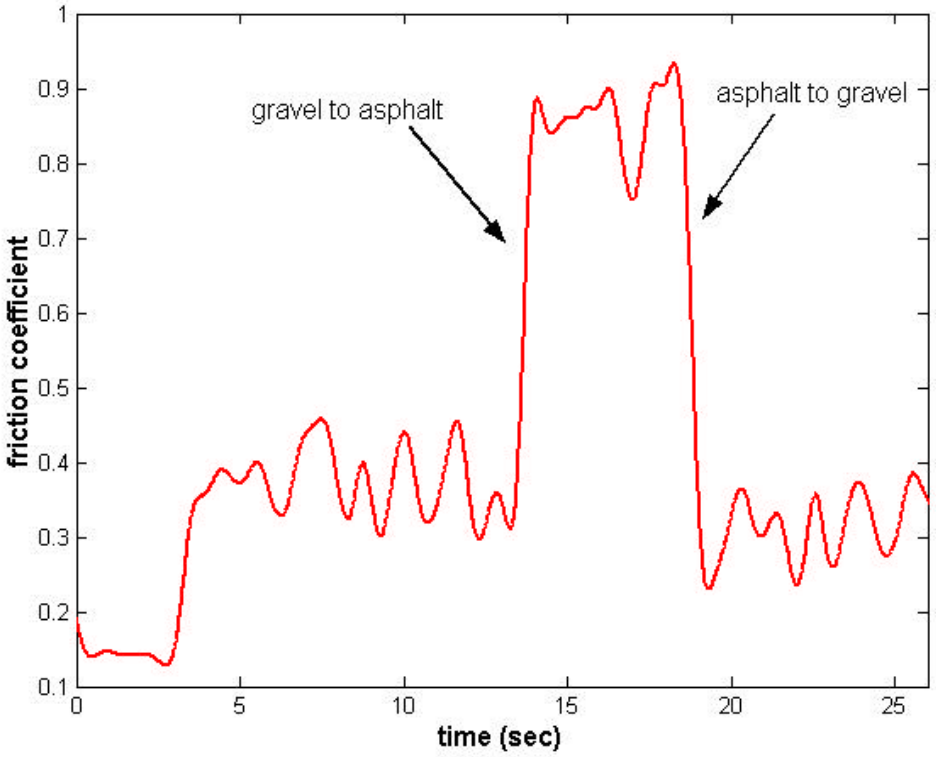

Figure 6.7 Friction coefficient in transitions from gravel to asphalt and vice-versa

Figure 6.6 show the measured friction coefficient on a gravel road close to the Maple Grove truck station. As seen in the figure, once the snowplow starts moving, the friction coefficient is measured to be a value around 0.4. This is clearly and significantly different from the value measured on dry asphalt.

Figure 6.7 shows the measured friction coefficient during transitions from gravel to dry asphalt and dry asphalt to gravel. As seen in the figure, the transition from one type of surface to another is measured very quickly. The friction coefficient changes quickly from 0.4 on gravel to around 0.85 on dry asphalt and then changes back to a value of around 0.4 on gravel.

Figure 6.6 can be compared to Figure 5.13 where the friction coefficient on gravel was earlier measured using the vehicle-based friction measurement system. Likewise, Figures 6.4 and 6.5 can be compared to the earlier results on dry concrete and dry asphalt in Chapter 5. It can be seen that the friction coefficient values measured by the friction wheel are in good agreement with the friction coefficient estimated by the vehicle-based system.

Chapter 7: Conclusions

This project concentrated on the development of real-time tire-road friction coefficient estimation systems for snowplows that can reliably estimate different road surface friction levels and quickly detect abrupt changes in friction coefficient. Two types of systems were developed – a vehicle-based system and a wheel-based system. The vehicle-based friction measurement system utilized vehicle motion measurements from differential GPS and other on-board vehicle sensors. The wheel-based friction measurement system utilized a redundant wheel that was mounted at a small angle to the longitudinal axis of the vehicle.

Complete technical details on the vehicle-based friction measurement system were presented in this report. Compared to previously published results in literature, the advantage of the vehicle-based system developed here is that it is applicable during both vehicle acceleration and braking and works reliably for a wide range of slip ratios, including high slip conditions. The system can be utilized on front/rear-wheel drive as well as all-wheel drive vehicles. Extensive results were presented from experimental results conducted on various surfaces with a winter maintenance vehicle called the "SAFEPLOW." The experimental results showed that the system performs reliably and quickly in estimating friction coefficient on different road surfaces during various vehicle maneuvers.

The new wheel-based system developed in this project has several advantages compared to the popular Norse-meter, which is a commercially available redundant wheel-based system. The new wheel-based system has very few moving parts, requires no actuators for skidding the wheel and requires no braking of the wheel. It is expected to be more reliable and much less expensive than the Norsemeter. Experimental results presented in this report showed that the new wheel-based system worked effectively in determining friction coefficient and in measuring the change of friction coefficient during transition from one type of surface to another.

The developed friction identification systems have many applications in vehicle safety systems such as ABS, skid control and collision avoidance systems and are also useful for winter maintenance vehicles in which knowledge of the friction coefficient can be used to determine the amount and type of deicing chemicals to be applied to a winter roadway.

References

[1] Bert Breuer, Ulrich Eichhorn, and J¨urgen Roth, “Measurement of tyre/road friction ahead of the car and inside the tyre,” *Proceedings of AVEC‘92 (International Symposium on Advanced Vehicle Control)*, pp. 347–353, 1992.

[2] U. Eichhorn, J. Roth, “Prediction and Monitoring of Tyre/Road Friction,” *Proceedings of FISITA*, London, 1992, pp. 67-74.

[3] T. Uno, Y. Sakai, J. Takagi, and T. Yamashita, “Road Surface Recognition Method Using Optical Spatial Filtering,” *Proceedings of AVEC*, 1994, pp. 509-515.

[4] SAE, “Vehicle Dynamics Terminology,” SAE J670e, Society of Automotive Engineers.

[5] W. R. Pasterkamp and H. B. Pacejka, “The Tyre as a Sensor to Estimate Friction,” *Vehicle System Dynamics*, vol. 27, 1997, pp.409-422.

[6] F. Gustaffson, “Slip-Based Tire-Road Friction Estimation,” *Automatica* Vol. 33 (6), pp1087-1099, 1997.

[7] K. Yi, K. Hedrick, and S. C. Lee, “Estimation of Tire-Road Friction Using Observer Based Identifiers,” *Vehicle System Dynamics*, vol. 31, p. 233-261, 1999.

[8] Wookug Hwang and Byung-suk Song, “Road Condition Monitoring System Using Tire-road Friction Estimation,” *Proceedings of AVEC 2000*, Ann Arbor, Michigan, pp 437-442, Aug. 2000.

[9] Steffen Müller, Michael Uchanski, and Karl Hedrick, “Slip-Based Tire-Road Friction Estimation During Braking,” *Proceedings of 2001 ASME International Mechanical Engineering Congress and Exposition*, New York, 2001, pp. 213-220.

[10] J.-O. Hahn, Rajesh Rajamani, and Lee Alexander, “GPS-Based Real-Time Identification of Tire-Road Friction Coefficient,” IEEE Transactions on Control Systems Technology, Vol 10, No. 3, May 2002.

[11] St. Germann, M. Würtenberger, and A. Daiß, “Monitoring of the Friction Coefficient Between Tyre and Road Surface,” *Proceedings of the third IEEE Conference on Control Applications*, pp. 613-618, 1994.

[12] Thomas D. Gillespie, “Fundamentals of Vehicle Dynamics,” Society of Automotive Engineers, Inc., 1992.

[13] Paul S. Fancher, Robert D. Ervin, Christopher B. Winkler, and Thomas D. Gillespie, "A Factbook of the Mechanical Properties of the Components for Single-Unit and Articulated heavy Trucks," The University of Michigan, Transportation Research Institute, Dec. 1986.

[14] Shankar Sastry and Marc Bodson, *Adaptive Control: Stability, Convergence, and Robustness*, Englewood Cliffs, NJ: Prentice-Hall, 1989.

[15] Fredrik Gustafsson, *Adaptive Filtering and Change Detection*, John Wiley & Sons, Ltd. Chichester, England, 2000.

[16] Thomas Kailath, Ali H. Sayed, and Babak Hassibi, *Linear Estimation*, Prentice Hall, 2000.

[17] E. S. Page, *Continuous Inspection Schemes*, Biometrika, vol 41, pp. 100-115, 1954.

[18] Rajesh Rajamani, "Radar Health Monitoring for Highway Vehicle Applications," *Vehicle System Dynamics*, Vol. 38, No. 1, pp. 23-54, 2002.

[19] D. Bevly, J Gerdes, C. Wilson, and G. Zhang, "The Use of GPS Based Velocity Measurements for Improved Vehicle State Estimation," *Proceedings of the American Control Conference*, Chicago, Illinois, pp. 2538-2542, June 2000.